

# HYDROGEN ADDITION TO FLAMES AT GAS-TURBINE-RELEVANT CONDITIONS

REPORT 2017:391



ENERGIGASTEKNIK





# Hydrogen Addition to Flames at Gas-Turbine-Relevant Conditions

ELNA J. K. NILSSON  
CHRISTIAN BRACKMANN  
ABDALLAH ABOU-TAOUK  
JENNY LARFELDT  
DANIEL MOELL

ISBN 978-91-7673-391-2 | © ENERGIFORSK May 2017

Energiforsk AB | Phone: 08-677 25 30 | E-mail: [kontakt@energiforsk.se](mailto:kontakt@energiforsk.se) | [www.energiforsk.se](http://www.energiforsk.se)



## Foreword

**This project evaluated how the combustion depend on fuel composition with respect to the components methane, ethane, propane and hydrogen. The results can contribute to more fuel flexible and environmentally sustainable production of electricity from gas turbines.**

**The report has been produced by Lund University, Chalmers University of Technology, Siemens Industrial Turbomachinery AB and the authors are Elna J.K. Nilsson (Lund University), Christian Brackmann (Lund University), Abdallah Abou-Taouk (Chalmers University of Technology), Daniell Moell (Siemens Industrial Turbomachinery AB) and Jenny Larfeldt (Siemens Industrial Turbomachinery AB).**

**The authors would like to acknowledge the Swedish Energy Agency, Energiforsk - Swedish Energy Research Center, for its financial contribution to the project within the scope of the program “Samverkansprogram Energigasteknik” – The cooperation research program Energy gas technology.**

**This work was also made possible by financial support from Siemens Industrial Turbomachinery AB, Infracore GmbH and Göteborg Energi AB.**

**The authors thank Moah Christensen, Jinlong Gao and Haisol Kim for help during experiments.**

**The study had a reference/working group with the following members: Jenny Larfeldt (Siemens Industrial Turbomachinery AB), Alexander Konnov (Lund University), Anton Fagerström (Energiforsk).**

Reported here are the results and conclusions from a project in a research program run by Energiforsk. The author / authors are responsible for the content and publication which does not mean that Energiforsk has taken a position.

## Sammanfattning

**Flammor av relevans för förbränning i gasturbiner har studerats med experiment och beräkningar. Målsättningen i projektet är att undersöka hur förbränningen beror på bränslesammansättningen med avseende på komponenterna metan, etan, propan och vätgas. Resultaten kan bidra till större bränsleflexibilitet och mindre miljöpåverkan vid elproduktion från gasturbiner.**

Förbränning av fossila bränslen behöver minskas, dels på grund av de resulterande klimatförändringarna men också för att de fossila bränslena är en ändlig energikälla. Det är fördelaktigt ur ekonomiskt och praktiskt perspektiv om elproduktionen framöver kan ske med samma teknologi som idag, men med förnybara bränslen. Stor del av världens elproduktion sker idag med gasturbiner som eldas med fossil naturgas. Under en övergångsperiod är det optimalt om en blandning av fossila och förnybara bränslen kan användas, med inga eller små förändringar i kraftverken. Därför är det ur ekonomiskt och samhällsperspektiv relevant att forska kring hur gasturbinförbränning kan ske med förnybara bränslen och olika bränsleblandningar.

En viktig framtida så kallad "energibärare" är vätgas, ett bränsle som kan produceras från en rad förnybara processer och som inte släpper ut några miljöfarliga komponenter vid förbränning. Vätgas är reaktiv och som nämns i rapportering av ett tidigare projekt Samledning med vätgas i industriella gasturbiner (SGC Rapport 2013:256) så stabiliseras flamman närmare brännarens utlopp vid höga vätgashalter. Publicerad forskning kring vätgasförbränning kan till viss del förklara de kemiska mekanismer som ligger bakom de förändringar i flamegenskaper som sker vid vätgasinblandning, men det saknas kunskap om vad som sker vid höga tryck samt hur effekterna kan variera beroende på sammansättning av kolvätena som vätgasen samledas med.

Framgångsrik förbränningsforskning innebär ofta en samverkan mellan laboratorieexperiment, idealiserade simuleringar av experimenten, mer avancerade simuleringar av applikationer, samt även fullskaleexperiment som det i den ovan nämnda rapporten. I innevarande projekt har laboratoriefloammar vid höga tryck karakteriserats och de experimentella resultaten har sedan jämförts med simuleringar för att ge en komplett bild av den bakomliggande kemien.

Den experimentella studien är utförd i en ny, unik, experimentuppställning och visar intressanta trender i flammornas karaktäristik, till exempel hur höjningen av flamhastighet som resulterar från vätgasinblandning motverkas av tryckökning. Viktiga resultat är undersökning av hur kinetiskmekanismer förutsäger flamegenskaper, jämfört med experimentella resultat. Överensstämmelsen med experimenten är över lag god, men avvikelserna är större för den kraftigt förenklade (4-steg) mekanism som utvecklats. Beräkningar innebär alltid en avvägning mellan tidsåtgång och tillförlitlighet, och resultaten i denna rapport kan utgöra vägledning i valet av beräkningsmekanism.

## Summary

**Flames of relevance to combustion in gas turbines have been studied using experimental and computational methods. The project aims at increasing the understanding of how the combustion depend on fuel composition with respect to the components methane, ethane, propane and hydrogen. The results can contribute to more fuel flexible and environmentally sustainable production of electricity from gas turbines.**

Combustion of fossil fuels is the main driver of climate change and should ideally be replaced by combustion of renewable fuels. In addition, the fossil fuels are a limited energy source. From economical and practical perspectives, it will be advantageous if production of electricity from renewable fuels can be done using the same base technology as today, which to a large extent mean using gas turbines. The dominating fuel today is fossil natural gas and during a transition period it would be ideal if fossil and renewable fuels could be co-fired. From economical and societal perspectives, research on fuel flexible gas turbines is therefore highly relevant.

An important future energy carrier is hydrogen gas, a fuel that can be produced from a range of renewable sources and has no combustion products that are of environmental concern. Hydrogen is a highly reactive compound, which has implications for its combustion characteristics. As mentioned in the report of an earlier project Sameldning med vätgas i industriella gasturbiner (SGC Rapport 2013:256) the flame is stabilized closer to the burner outlet at high hydrogen fractions. Published research about hydrogen combustion can to some extent explain the chemical processes underlying the changes in flame properties, but there is a lack of knowledge about the processes at elevated pressures and how the effects vary depending the composition of the hydrocarbon fuel the hydrogen is co-fired with.

Combustion research often rely on laboratory experiments, modeling of the experiments, modeling of more advanced applications, and full scale experiments as the one mentioned above. The present project employ studies of laboratory flames at elevated pressures, and simulations at different levels of complexity, to access details on flame characteristics as well as the fundamental chemical details.

The experimental studies conducted in a new, unique, setup reveal interesting trends in flame properties, an important example is that the increase in laminar burning velocity is counteracted by elevation of pressure. Important results are an evaluation of chemical kinetics mechanisms at different levels of complexity, and their validation against experimental results. The studied mechanisms all reproduce experimental cases fairly well, but the important point is the relation between accuracy and computational time.

## List of content

<b>1</b>	<b>Background</b>	<b>8</b>
1.1	Introduction	8
1.2	Gas turbine combustion	9
1.3	Hydrogen as a gas turbine fuel	9
1.4	Combustion research: challenges and approaches	10
1.5	Purpose and aims	11
1.6	Structure of report	12
<b>2</b>	<b>Experiments</b>	<b>13</b>
2.1	Overview of experimental approach	13
2.2	High-pressure burner setup	13
2.3	Raman spectroscopy	14
2.3.1	General theory	14
2.3.2	Challenges in combustion applications	15
2.3.3	Experimental configuration	15
2.4	Laser-induced fluorescence	16
2.5	Burning velocity determination	17
2.6	Experimental conditions	18
<b>3</b>	<b>Laminar flames: Simulation methods</b>	<b>20</b>
3.1	Introduction	20
3.2	Kinetic mechanisms	21
3.3	Methodology for development of global mechanism	22
3.4	CFD of laminar flames	24
3.4.1	Method	24
3.4.2	Boundary conditions and evaluation planes	25
<b>4</b>	<b>Laminar flames: Results and discussion</b>	<b>26</b>
4.1	Detailed kinetic simulations of 1D flames	26
4.2	Performance of a global mechanism	27
4.3	CFD simulations methane/air flames	30
4.3.1	Contour plots	30
4.3.2	Temperature and velocity profiles	31
4.3.3	Species concentration profiles	32
4.4	CFD simulations: Variation of H <sub>2</sub> concentration	34
4.5	Experimental results	35
4.5.1	Laminar burning velocity	35
4.5.2	Species concentration profiles: Hydrocarbon combustion	37
4.5.3	Species concentration profiles: Hydrogen addition	39
<b>5</b>	<b>Simulation of industrial burner</b>	<b>42</b>
5.1	Method	42
5.2	Results and discussion	43

5.2.1	Real engine case without hydrogen addition	43
5.2.2	Atmospheric case with hydrogen addition	44
<b>6</b>	<b>Conclusions</b>	<b>45</b>
6.1	Summary of main results	45
6.2	Implications for gas turbine combustion	45
6.3	Outlook	46
<b>7</b>	<b>References</b>	<b>47</b>
	<b>Appendix A</b>	<b>50</b>
	<b>Appendix B</b>	<b>64</b>
	<b>Appendix C</b>	<b>65</b>

# 1 Background

*“The Stone Age did not end because we ran out of stones; we transitioned to better solutions”*

- Chu and Majumdar (Nature, 2012) [1]

## 1.1 INTRODUCTION

The citation above is a hint at the necessary way to approach a sustainable future energy supply. Chu and Majumdar [1] point at the fact that our ability to extract fossil fuels in combination with the demand will keep the use of these fuels high for many decades into the future. A transition into renewable energy production depends on that the new solutions are as good as, or better than, fossil fuels, from technical and economical perspectives. A way to keep the need for financial investments low is to enable implementation of renewable energy production using the same facilities as used for fossil fuel combustion. For example, by operating gas turbines, that today mainly burn natural gas, on renewable fuels or mixtures of fossil and renewable fuels. This will demand fuel flexibility, which motivates investigations on how current gas turbines perform with different fuel combinations.

The main component of fossil natural gas is methane,  $\text{CH}_4$ , but composition varies with respect to amount of heavier hydrocarbons (ethane  $\text{C}_2\text{H}_6$ , propane  $\text{C}_3\text{H}_8$ , butane  $\text{C}_4\text{H}_{10}$ ), less reactive species as  $\text{CO}_2$ , and highly reactive hydrogen gas,  $\text{H}_2$ . Fuel flexibility is an important concern already today since new natural gas fields are exploited and variations in gas composition are expected to increase, which mean that gas turbines fueled from the natural gas grid can be subject to large day-to-day variations in energy content of the fuel, as previously reported in Energiforsk Report 2015:121 [2]. These fluctuations can result in unstable operating conditions affecting the output of energy and in extreme cases potentially trigger hazardous events as a result of flame extinction or flashback in the burners.

Renewable sources of gaseous fuels are waste- or process gases from industry, for example propane or hydrogen, that can be used as gas turbine fuels instead of being released or flared. Biogas from gasification of bio material is another renewable energy solution, in Sweden exemplified by the GoBiGas facility in Gothenburg<sup>1</sup>. An example of use of an industrial product gas is the chemical and pharmaceutical site Industriepark Höchst in Frankfurt am Main, Germany, operated by Infracore GmbH<sup>2</sup> & Co. Höchst KG2, where hydrogen is produced as a by-product from the chemical industry. In future, the hydrogen gas generated by electrolysis from renewable energy sources is an environmentally friendly source of energy that can be mixed with the natural gas if the gas turbine is designed to handle the combustion properties of this highly reactive gas mixture. At the

<sup>1</sup> [http://gobigas.goteborgenergi.se/English\\_version/Start](http://gobigas.goteborgenergi.se/English_version/Start)

<sup>2</sup> <http://www.infracore.com/en/index.jsp>

Industriepark Höchst site a mixing station for up to 15% hydrogen gas is under construction, this is reported in Appendix A of this report.

Hydrogen is also relevant to consider as an energy carrier since it can store energy from (i.e. be produced from) a wide range of energy sources: extraction from fuels, electrolysis, wind-, solar- and hydropower. With these multiple production routes hydrogen can play a role in balancing the energy need, produced when sources provide surplus energy and combusted to produce additional energy when demand is high.

## 1.2 GAS TURBINE COMBUSTION

Gas turbines are important devices for electricity production worldwide and due to their fast startup procedure and load flexibility, they are suitable to combine with solar or wind power for energy supply at peak demand [1]. Combustion properties of importance for gas turbine combustion are the laminar burning velocity (also called burning velocity) and the ignition delay time. The former quantifying the speed at which a flame propagates in a premixed combustible mixture, and the latter the time it takes for the gas mixture to auto ignite. These combustion characteristics are dependent on temperature and pressure [3], for each unique gas mixture composition with respect to fuel components, oxygen content and amount of inert gas. Gas turbine combustion operates under conditions that on the low-reactivity side are limited by flame blowout, or extinction, at conditions where combustion can no longer be sustained, and on the high-reactivity side by flashback of the flame too far upstream in the burner or fuel supply system [4]. Design of fuel-flexible gas turbines requires understanding of how variation in gas mixture composition will affect the combustion characteristics over the range of pressures and temperatures encountered in the system. For example; combustion of a highly reactive fuel might require a particular design of the burners or gas feeding systems to prevent flashback upstream of the position where the flame should be anchored to optimize energy production.

## 1.3 HYDROGEN AS A GAS TURBINE FUEL

Hydrogen is considered a promising future gas turbine fuel; it is available from a range of sources and its combustion does not release any harmful green-house gases contributing to global warming. When added to natural gas or other hydrocarbon fuels it can act as a combustion enhancer; mixed in appropriate amounts it enhances the reactivity of the gas, increases the flammability range, and thus result in more stable combustion [5, 6]. A controlled feeding of hydrogen gas can be used as a mean to counteract variations in gas composition and give more stable operation of a gas turbine, as proposed previously by the authors [2].

Characteristics of hydrogen flames have been reviewed by Sanchez and Williams [13], who point out that the understanding is still insufficient, in particular at high-pressure conditions valid for real combustion systems. Research on combustion of hydrogen mixed with hydrocarbons was reviewed by Tang et al. [14]. Flames of methane/air with hydrogen addition are well studied and the increase in laminar burning velocity can be divided into three regimes [14]. Up to 60% hydrogen

content the increase in laminar burning velocity with increased hydrogen fraction is modest and the chemistry is considered to be hydrocarbon dominated, this range is covered in Fig. 1a, from Nilsson et al. [7], where laminar burning velocity is plotted versus hydrogen fraction. At the highest hydrogen levels (>90%) the increase in laminar burning velocity is dramatic, showing that the chemistry is rapidly becoming hydrogen dominated. The intermediate regime, when the hydrogen fraction is in the range 60-90%, shows an intermediate behavior.

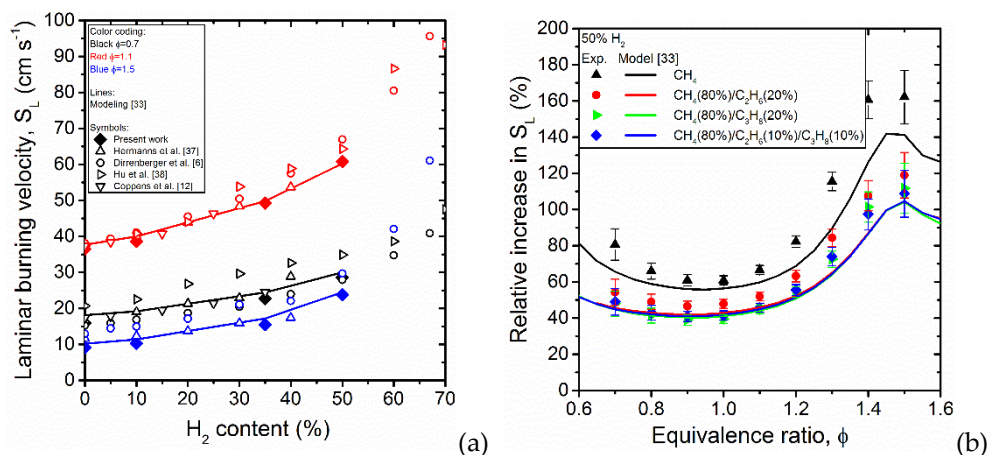


**Figure 1. Laminar burning velocities for flames at atmospheric pressure and initial gas temperature of 298 K. Figures from Nilsson et al. [7]. a)  $S_L$  as a function of H<sub>2</sub> content for three equivalence ratios, including data from several experimental studies [7-11], and b) relative increase in  $S_L$  as a result of 50% H<sub>2</sub>, for various hydrocarbon mixtures [7]. Solid lines represent modeling [12].**

Experiments on butane/hydrogen/air, in combination with kinetic modeling, indicate that the combustion enhancement effect resulting in increased laminar burning velocity,  $S_L$ , is larger for methane compared to the heavier hydrocarbon [15]. A similar conclusion is drawn by Brower et al. [16] based on a modeling study; a natural gas mixture with about 20% heavier hydrocarbons is less affected by hydrogen addition compared with a methane flame. For atmospheric pressure flames the modeling results by Brower et al. were confirmed experimentally by Nilsson et al. [2, 7], Fig. 1. From Fig. 1b it is evident that increase in laminar burning velocity is smallest around stoichiometric conditions, which mean close to the maximum in  $S_L$ , while the effect increases towards lean and rich conditions. Also, in Fig. 1b it is clear that methane is more affected by hydrogen addition than the mixtures with heavier hydrocarbons.

#### 1.4 COMBUSTION RESEARCH: CHALLENGES AND APPROACHES

Successful research on combustion characteristics is a combination of experimental and modeling studies [17]. Experimental determination of a combustion property like flame propagation can be modelled using chemical kinetics schemes to reveal the underlying chemical reactivity. For combustion chemistry research purposes, laminar 1-dimensional (1D) flames are often studied since they are simple enough to be modelled with a high chemical detail [18]. From an experimental point of view one of the significant challenges is to design experiments at relevant conditions with respect to temperature, pressure and gas mixture composition. The

challenge is twofold since first a stable flame configuration has to be achieved, then suitable diagnostic tools have to be applied to investigate it. To transfer the knowledge gained from experimental and computational studies of laminar flames to the turbulent combustion of real-world applications like gas turbines, more complex simulations using Computational Fluid Dynamics (CFD) are required.

The modeling challenge in turbulent reacting flows of turbulent flames has been the subject of numerous studies [19-26] and arises from complex interactions between the turbulent flow field, flame reactions, and combustor geometry. A fundamental understanding of the underlying mechanisms has not fully been reached so far, and further experimental and numerical studies are necessary. In recent years, detailed laser diagnostic studies in industrial and laboratory flames have contributed significantly to a better understanding of processes such as flame stabilization, combustion instabilities and finite-rate chemistry effects. As for example in a study by Lantz et al. [5] investigating hydrogen enrichment in gas turbine burners. However, industrial gas turbine combustors are complex to investigate experimentally because of many challenges, such as optical access, complexity of design, and difficulty to iterate through design changes. CFD simulations are valuable as tools for design and evaluation of real combustors, by being comparably cheap and bringing detailed understanding of processes that cannot be experimentally studied.

In the present work laboratory experiments are coupled with 1D simulations to gain detailed knowledge on flame chemistry. In addition, flames are modelled using CFD simulations.

## 1.5 PURPOSE AND AIMS

The overall purpose of the project is to improve the understanding of co-firing with hydrogen in hydrocarbon flames, at conditions relevant for gas turbine combustion. Fundamental understanding of flame composition was investigated experimentally and computationally. A simplified computer model for combustion simulations was developed and its validity was tested using experimental data and modeling on a higher level of chemical detail. To achieve the overall goal, three sub goals were defined:

1. Experimental characterization of flames stabilized at high pressures. Composition with respect to hydrocarbons were varied by addition of 20% ethane and/or propane to methane fuel. In addition, methane and methane/ethane were co-fired with up to 35% H<sub>2</sub>.
2. Simulation of the flames using detailed chemical kinetics models to achieve understanding of the reactivity. The full range of pressures visited in the experiments were covered. The different hydrocarbon mixtures were modelled, as well as co-firing with up to 80% hydrogen.
3. Validation and improvement of simplified kinetics models and their application to turbulent combustion of relevance to gas turbines.

## 1.6 STRUCTURE OF REPORT

The experimental setup, diagnostics tools and analysis methods are outlined in section 2, with a focus on the novel or unique aspects of particular importance to the present experiments. Simulations at different levels of complexity are employed in this project and an overview of this is given in beginning of section 3, followed by more detail on the methodology for development of a global reaction mechanism, and the specific characteristics describing modeling of the experimental setup. Results for laminar flame studies in section 4 are divided into three main parts: expected trends in reactivity of the fuel mixtures obtained from modeling of 1D flames; performance of mechanisms of different levels of complexity when modeling the experimental configuration; and finally the experimental results are presented and discussed in relation to the modeling results. Section 5 present simulations of gas turbine cases using a global mechanism of the type developed within the project. In a final section main results are summarized and important implications for gas turbine combustion are explained.

## 2 Experiments

### 2.1 OVERVIEW OF EXPERIMENTAL APPROACH

Laminar premixed flames are stabilized on a circular burner nozzle enclosed in a high-pressure vessel, Fig. 2a, where pressure and flame composition can be varied continuously during an experiment [27], further information is given in Section 2.2. The vessel is equipped with windows for optical access that allow laser-based diagnostic methods to be used for non-intrusive measurements of flame structure, i.e. distribution of chemical species in flames.

At elevated pressure the flame structure is compressed, which presents a challenge since measurements need to be made with sufficient spatial resolution to distinguish regions of reactants and combustion products. Moreover, increased number of molecular collisions at elevated pressure makes signal quantification complex for many techniques. In the present work flame structure was investigated using Raman spectroscopy, which allows for measurement with high spatial resolution and provides an instantaneous signal independent on molecular collisions. In addition, the technique allows for simultaneous measurement of multiple species.

The drawback of Raman Spectroscopy for combustion diagnostics is the generally weak signals due to the low probability of the intrinsic scattering process. To overcome this and get the best possible sensitivity for species concentration measurements a high-power high-repetition-rate Nd:YAG laser was used, with the beam arranged for dual passage through the high-pressure burner vessel. The Raman signal has been optimized by collection through optical windows on both sides of the measurement region. A high-quality optical filter was used for suppression of scattered laser light for collection of background-free Raman data, facilitating evaluation of quantitative species concentrations. The general theory as well as specific details on the Raman setup used for the present project are outlined in Section 2.3.

### 2.2 HIGH-PRESSURE BURNER SETUP

A versatile high-pressure vessel intended to host different burners, and suited to study both premixed and non-premixed flames, has been constructed at the Division of Combustion Physics [27]. The vessel, see Fig. 2, has an inner volume of 25 liters, can be operated at pressures up to 35 atmospheres and temperatures up to 220°C. The pressure can be varied over short time to enable direct comparisons of results obtained at different pressures over a single measurement period. Optical access is provided through four windows, allowing for optical diagnostics from deep ultraviolet to mid-infrared wavelengths.

The assembly of the burner is visible in Fig. 2b showing a normal co-flow burner with a long tube in the center that carries the combustible gas and acts as a flame anchor. The outside diameter of the central burner tube is 10 mm and the inside diameter is 7 mm.

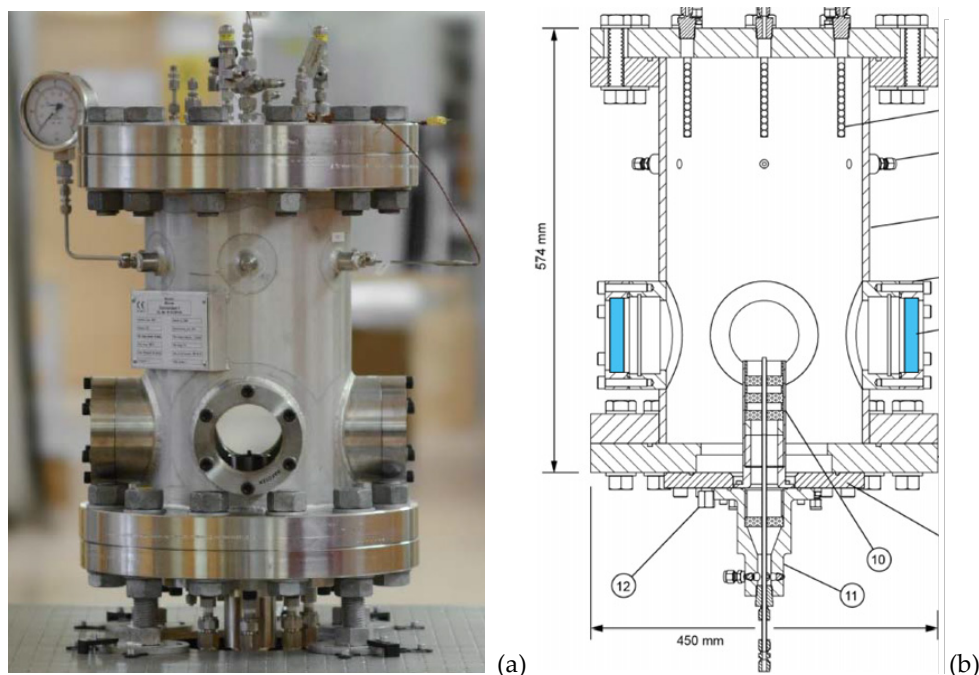


Figure 2. High-pressure burner setup [27], a) pressure vessel, and b) a general schematic of the pressure vessel and with interchangeable burner module.

## 2.3 RAMAN SPECTROSCOPY

### 2.3.1 General theory

Raman spectroscopy is based on spontaneous Raman scattering, an inelastic scattering of laser photons in which energy is transferred via vibrating and rotating molecules. The energy of the Raman-scattered photons is species specific as it is determined by the molecules interacting with the incident laser photons. The Raman scattering process is simultaneously induced in several different species and acquisition of Raman spectra provides multi-species detection; however, the probability for the interaction is low resulting in weak signals, which limits species detection sensitivity.

The background physics of Raman spectroscopy in the context of combustion diagnostics is described in the textbook by Eckbreth [28] and guidance for an experimental design has been presented by Miles [29]. Using the notation of Miles, the number of scattered Raman photons,  $S_{\text{Raman}}$ , for a species in a given probe volume is given by Eq. (1).

$$S_{\text{Raman}} = \frac{E_{\text{laser}} \left( \frac{\partial \sigma}{\partial \Omega} \right) X N \Omega l \eta}{h \nu_{\text{Raman}}} \quad (1)$$

In Eq. (1)  $E_{\text{laser}}$  is the incident laser energy in the probe volume and  $(\partial \sigma / \partial \Omega)$  is the differential Raman cross section for the species, representing the probability of inducing the scattering process. The species concentration is given by the product of the species mole fraction  $X$  and the total gas number density  $N$ . The geometrical signal collection is given by the solid angle  $\Omega$ ,  $l$  is the probe volume length,  $\eta$  is a detection efficiency,  $h$  Planck's constant and  $\nu_{\text{Raman}}$  is the frequency of the scattered

photons. Equation (1) gives that the number of scattered photons is proportional to the species concentration ( $X$ ) by the laser energy and the cross section. To achieve a detectable signal for species with a low cross section the experimental design will benefit from a high laser energy and a high concentration of species.

### 2.3.2 Challenges in combustion applications

Important challenges for using Raman spectroscopy in combustion applications are the short time scales of the phenomenon and the need for spatial resolution. The laser energy deposited in the probe-volume is determined by the average power and the measurement time. For combustion diagnostics rather short measurement times are desirable, either due to high continuous background luminosity from the flame and/or non-stationary conditions in turbulent reactive flows. Pulsed lasers, emitting high energy during a short period of time, typically ten nanoseconds, are advantageous for this purpose. In addition, it is desirable to make measurements of flame structure with high spatial resolution, typically sub-mm scale for atmospheric pressure flames, which is achieved using focused laser beams. However, delivering energy under such conditions to generate a sufficient number of detectable Raman photons, the laser irradiance (unit  $W/m^2$ ) often exceeds the threshold for laser-induced electric breakdown in the probed gas, which is on the order of  $10^{12} W/cm^2$  and sets a limit on the energy that can be employed in a single laser pulse.

While turbulent conditions require measurements on a very short time scale using single laser pulses, this is not required for steady-state laminar flames investigated in the present study. High-repetition-rate kHz laser systems with average powers on the order of 100 W have opened up additional possibilities for Raman spectroscopy. With the laser energy distributed over a large number of pulses per second, high average power can be used while maintaining sufficiently low power in each pulse to avoid electric breakdown. Using such a laser, measurements at high average power can thus be achieved by acquisition over multiple pulses.

Further Raman signal enhancement can be achieved by arranging for multiple passages of the laser pulse through the measurement volume, thus increasing the incident energy by a factor equal to the number of passages. Multi-pass configurations allowing for more than 100 passages have been successfully implemented for Raman spectroscopy, for example by Utsav et al. [30].

### 2.3.3 Experimental configuration

The experimental setup for the Raman spectroscopy on flames in the high-pressure vessel is schematically drawn in Fig. 3.

To achieve high average laser power a high-repetition-rate diode-pumped Nd:YAG laser (HD40I-OE, Edgewave) that can be operated from emission of single pulses up to a repetition rate of 20 kHz, was used. The laser pulse duration is 12 ns and the second harmonic beam at wavelength 532 nm used for Raman spectroscopy provides a pulse energy of 12 mJ at a repetition rate of 10 kHz resulting in an average power of 120 W. The experimental setup is shown in Figure

2, where the 532 nm laser beam is guided back and forth through the high-pressure burner vessel using dichroic mirrors (DM).

As explained in the previous section, a multi pass configuration can be used to improve the signal. However, in the present setup the thick windows subject to high pressure in the vessel as well as limited possibilities to observe the beam passage in the measurement volume makes alignment of multiple beam passages challenging. A dual passage of the laser beam has therefore been arranged.

The optical configuration of the setup, Fig. 3, can be described as follows: prior to entering the vessel, the beam is focused above the burner using a spherical lens ( $L_1$ ) of focal length  $f=300$  mm. A second  $f=300$  mm lens ( $L_2$ ) re-collimates the beam as it exits the burner and then refocuses it as it again enters the burner and propagates in the opposite direction. The beam then exits through the entrance window, is re-collimated using lens  $L_1$ , and terminated by a beam dump. The Raman signal is collected perpendicular to the beam path through a window by a pair of achromatic lenses ( $L_3$ ) of focal length  $f=200$  mm and imaged on the entrance slit of a spectrometer of focal length  $f=150$  mm (Acton SpectraPro SP-150, grating 1200 grooves/mm). In addition, Raman signal scattered in the direction opposite to the detector side is reflected towards the detector using a spherical mirror (SM). A filter (Semrock, BLP01-532R-25) is used for suppression of scattered laser light.

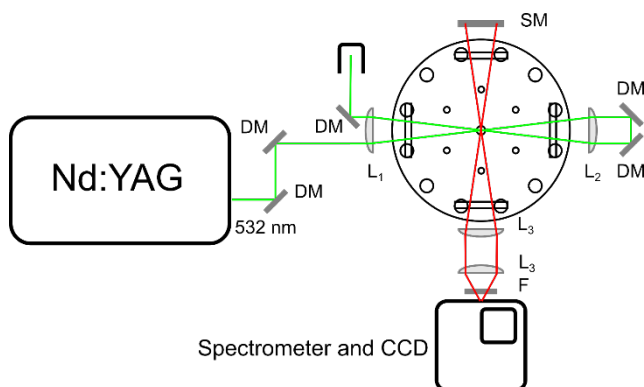


**Figure 3. Experimental setup for Raman spectroscopy in high-pressure burner using the 532 nm beam (green) from an Nd:YAG laser. Abbreviations: DM- dichroic mirror, L – lens, SM – spherical mirror, F – detection filter. The path of the Raman signal collected to the spectrometer is indicated by the red rays.**

## 2.4 LASER-INDUCED FLUORESCENCE

Laser-induced fluorescence (LIF) is a technique that allows for highly sensitive, down to sub-ppm levels, detection of minor species in flames, see for example ref. [31] and references therein. The method is based on excitation via resonant absorption of laser photons and detection of spontaneously emitted fluorescence. The wavelengths of the emitted fluorescence are usually different than that of the laser, which is advantageous for background-free detection. While the list of qualitative studies using LIF is extensive, combustion studies with quantitative species concentrations measured with LIF are scarce due to challenges in converting measured signals into absolute species concentrations. The impact of molecular collisions, quenching, is most challenging to deal with in this context since they are dependent on conditions such as chemical composition, temperature, pressure, and the quantum states involved. It is, however, possible to

account for collisional quenching by measuring concentrations of major species and temperature, from which collisional quenching rates can be determined using quenching cross section data. Major species concentrations and temperature can be obtained by Raman spectroscopy as outlined above and combined Raman/LIF measurements have been demonstrated [32].

Nevertheless, also qualitative LIF measurements can provide valuable information, in particular by visualization of species distributions in imaging measurements. This has for example been employed in studies of flame front propagation.

For the flames investigated in this project the reaction-zone has been visualized by LIF imaging of the CH radical distribution [33]. While this species partly accounts for the flame chemiluminescence appearing in a normal photo, background free LIF images of CH only, provide a more accurate determination of the reaction zone position allowing for comparison and determination of laminar burning velocity, as presented in the following section. In these experiments, a solid-state Alexandrite laser at wavelength 387 nm has been employed for CH excitation, while the laser beam was shaped into a thin vertical focused sheet propagating through the center of the flame. Images of CH distributions in the laser sheet were obtained using the CCD detector equipped with a Nikon camera lens and an optical filter (Schott, GG400).

## 2.5 BURNING VELOCITY DETERMINATION

The laminar burning velocity,  $S_L$ , is a quantity of fundamental interest for premixed combustion. For a premixed flame stabilized at the orifice of a tube supplying the premixed fuel and oxidizer, i.e. a Bunsen-type burner, the burning velocity can be estimated from the shape of the flame cone. For a stable stationary flame as shown in the photo of Fig. 4 the flow speed,  $v$ , of the unburned reactant mixture and the laminar burning velocity  $S_L$  is given by Eq. (2).

$$S_L = v \cdot \sin(\alpha) \quad (2)$$

Where  $\alpha$  is the half top angle of the flame cone. In the photo of Fig. 4, the flame cone is defined by the reaction zone emitting bright blue flame chemiluminescence from excited molecular CH radicals.

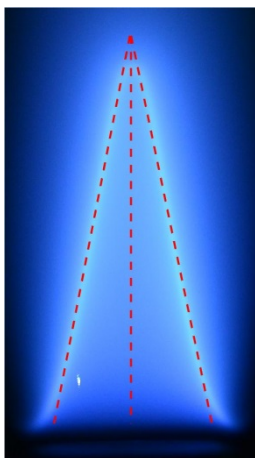


**Figure 4. Photo of stoichiometric CH<sub>4</sub>-air flame at atmospheric pressure. The flame cone is defined by the reaction zone emitting bright blue flame chemiluminescence from excited molecular CH radicals.**

An evaluation routine was developed to fit straight lines to the shape of the flame cone, as indicated by the red dashed lines in Fig. 4, and in turn determine the cone angle  $\alpha$ . Together with flow speeds determined from the mass-flows of fuel and air (cf. Table 1) this allowed for calculation of  $S_L$ . This is considered a rather crude method for estimation of  $S_L$ , less accurate than for example the Heat Flux method used in a previous study [7]. That method is, however, not applicable to the present high pressure studies, where the Bunsen flame has to be used. In the present project the main focus is, however, not the absolute value of the laminar burning velocity, but rather the change with pressure and gas composition. Therefore, a consistent treatment of the data is the important factor, to allow for comparison of results at different conditions. Nevertheless, for atmospheric pressure flames obtained values can be compared with values determined using more accurate methods in order to assess the accuracy of this method.

## 2.6 EXPERIMENTAL CONDITIONS

Gas mixtures were purchased from AGA, premixed bottles with hydrocarbon composition CH<sub>4</sub>/C<sub>2</sub>H<sub>6</sub>/C<sub>3</sub>H<sub>8</sub> of 100/0/0, 80/20/0, 80/0/20 and 80/10/10 by mole%. The CH<sub>4</sub> and the CH<sub>4</sub>/C<sub>2</sub>H<sub>6</sub> mixtures were in addition mixed with H<sub>2</sub> to 10, 25, and 35%. Experimental conditions are summarized in Table 1.

Experiments were performed by setting a target gas mixture composition at a particular velocity using mass flow controllers, at atmospheric chamber pressure. The velocity and pressure was then varied to visit different conditions, which allowed adjustment of flame height to get optimal conditions for the optical diagnostics.

Table 1. Gas mixtures and experimental parameters investigated.

Composition	$\phi$	P (atm.)	Velocity (cm/s)	Composition	$\phi$	P (atm.)	Velocity (cm/s)
CH <sub>4</sub>	0.9	1	115	CH <sub>4</sub> + 35% H <sub>2</sub>	0.9	1	155
	0.9	1	90		0.9	2	166
	0.9	1	80		1.0	1	175
	1.0	1	145		1.0	2	133
	1.0	2	113		1.2	1	168
	1.0	3	99		1.2	2	122
	1.1	1	143		1.2	3	98
	1.1	2	110		1.3	1	160
	1.1	3	93		1.3	2	108
	1.1	4	81		1.3	3	82
	1.2	1	123		1.3	5	65
	1.2	2	93		1.4	1	127
	1.2	3	68		1.4	2	70
	1.2	4	59		CH <sub>4</sub> 20% C <sub>2</sub> H <sub>6</sub>	0.9	1
	1.2	5	52	0.9		2	90
	1.2	6	45	1.0		1	145
	1.3	1	115	1.0		2	118
	1.3	2	85	1.0		3	110
	1.3	3	60	1.1		1	143
	CH <sub>4</sub> + 25% H <sub>2</sub>	0.9	1	198		1.1	2
0.9		2	151	1.1		3	105
0.9		3	126	1.2	1	123	
1.0		1	173	1.2	2	93	
1.0		2	137	1.2	3	78	
1.0		3	130	1.2	4	75	
1.2		1	150	1.3	1	107	
1.2		2	112	1.3	2	80	
1.2		3	90	1.3	3	60	
1.2		5	66	1.3	4	55	
1.4		1	116	1.3	5	50	
1.4		2	73	1.3	6	45	
1.4		3	52	1.3	7	43	
					1.3	8	40

### 3 Laminar flames: Simulation methods

#### 3.1 INTRODUCTION

A chemical kinetic mechanism of a combustion process includes chemical reactions, each represented by three parameters,  $A$ ,  $E_a$  and  $n$ , to capture the temperature dependence using the Arrhenius equation:

$$k = A T^n e^{\frac{-E_a}{RT}} \quad (3)$$

For many reactions an even higher complexity is required to describe the pressure dependence. Detailed kinetic mechanisms with all possible reaction paths over a wide temperature and pressure range are used for modelling of simplified laboratory systems like flat, laminar flames. This type of modelling can give deep insights in the underlying chemistry and is essential for fundamental understanding of combustion chemistry. These mechanisms are, however, far too computationally expensive for simulations of turbulent combustion. To minimize computational time global kinetic mechanisms are commonly used, where fuel breakdown to formation of final products carbon dioxide and water are represented by one to five steps. This simplified approach is sometimes necessary, but is of course a crude approximation, in particular for larger hydrocarbon fuels with several carbon atoms. Intermediate-sized schemes, named reduced or skeletal mechanisms, of tenths to hundred reactions are a trade-off between the detailed and global approaches [34]. The span of numbers of reactions in the mechanisms are represented in Fig. 5.

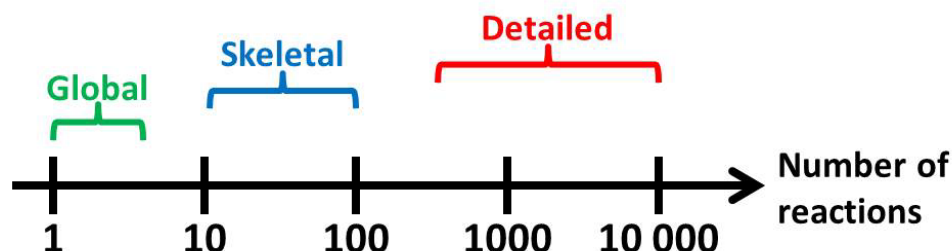


Figure 5. Size span, based on number of reactions, for the mentioned types of kinetic reaction schemes.

There is a high demand on the computational and theoretical combustion modelling community to develop and deliver tools and methodologies that can be used in the process of reducing the computational cost of combustion simulations. In order to reduce the computational cost of flame simulations, several methods have been developed during the last decades, which simplify the description of the reaction kinetics. Most of these methods are based on partial-equilibrium and steady-state assumptions, assuming that most chemical processes have a much smaller time scale than the flow. Chemistry reduction has also been previously addressed by providing strongly reduced chemical mechanisms [35-45] or using chemical lookup tables obtained either from low dimensional manifold projection [46] or from one- or multi-dimensional canonical combustion problems [47, 48].

The use of global reaction mechanisms involving a limited number of species is of practical interest, specifically when dealing with complex burner geometries in industrial applications featuring multiple inlets, dilution with burnt gases in recirculation zones and heat losses. In these complex flow situations, the full tabulation of chemistry may become complex because of the number of control parameters (fuel, oxidizer, dilution, heat losses, etc.), which are necessary to parameterize in the look-up table.

In this work, using well-established optimization tools, the parameters of a four-step reduced mechanism for methane-hydrogen-air chemistry are determined from a set of reference detailed chemistry solutions. The optimization is performed so that the balance equations of the species mass fractions and temperature involved in the reduced mechanism, reproduce the detailed chemistry solution. An objective of the present work is to create a reduced mechanism for premixed methane-hydrogen-air combustion.

In this section the theory and methodologies used for combustion simulations within the present project, are introduced. First some background on the chemical kinetics schemes is given, followed by a section on the methodology used to reduce the detailed mechanism to give a mechanism useful for CFD simulations. Finally, details related to the CFD simulations are outlined.

### 3.2 KINETIC MECHANISMS

Several kinetic mechanisms of different complexity are used in the present study. For 1D flame simulations the highly detailed Aramco 1.3 [12] mechanism is employed, a mechanism that has been thoroughly validated over a wide range of conditions, and probably is one of the most accurate of detailed mechanisms available today. GRI-Mech 3.0 [49] is popular in the CFD community since it is fairly small and computationally efficient, while still in agreement with experimental data over a range of conditions. Z42 [17] is a new reduced mechanism building on a reduction method where the fuel breakdown reactions are simplified, while more detail is kept in the base mechanism, an approach that has proved to be successful for several fuels [34]. The four step global mechanism developed in the present work, see Section 3.4, is using GRI-Mech 3.0 as a starting point.

**Table 2.** Kinetic mechanisms used in the present study.

Mechanism	Species	Reactions	Fuels	Reference
Aramco 1.3	171	1140	H <sub>2</sub> , C1-C3 hydrocarbons	[12]
GRI-Mech 3.0	32	177	H <sub>2</sub> , C1-C3 hydrocarbons	[49]
Z42	18	42	CH <sub>4</sub> , H <sub>2</sub>	[17]
Present four-step	7	4	CH <sub>4</sub> , H <sub>2</sub>	

### 3.3 METHODOLOGY FOR DEVELOPMENT OF GLOBAL MECHANISM

The choice of species and reactions for a global mechanism is not straightforward, the four reactions selected for the present mechanisms are presented in Table 3: (i) the fuel oxidation into CO and H<sub>2</sub>; (ii) H<sub>2</sub> and O<sub>2</sub> into H<sub>2</sub>O, (iii) CO and O<sub>2</sub> into CO<sub>2</sub>; and (iv) the water gas shift reaction, CO and H<sub>2</sub>O into CO<sub>2</sub> and H<sub>2</sub>. The forward reaction rates (R1-R4) are shown below. The backward reaction rates are based on equilibrium constants.

In a detailed reaction mechanism, the rate parameters involved in elementary reactions have physical meaning and are validated with experimental data. However, global mechanisms usually have no such direct physical meaning, but rely on fitting reaction parameters to achieve certain target predictions such as burning velocity, species concentration and temperature profiles. The most common optimization approach, once the global mechanism is defined in terms of species, reactions, rate-controlling parameters and target data, is to apply a multi-objective procedure to find the best values for these parameters. The target data are obtained from detailed chemistry calculations, for example from 1D laminar flame computations where thermal diffusion was included. In this work the GRI-Mech 3.0 [49] is used as a reference mechanism.

Table 3. Kinetic rate data (units in cm, s, kcal and mol)

	Present scheme	A	Ea	B
1	CH <sub>4</sub> + 0.5O <sub>2</sub> → CO + 2H <sub>2</sub>	2.06E14	38.25	-0.1
2	H <sub>2</sub> + 0.5O <sub>2</sub> ↔ H <sub>2</sub> O	2.656E18	40.50	-0.8
3	CO + 0.5O <sub>2</sub> ↔ CO <sub>2</sub>	2.96E14	44.25	-0.1
4	CO + H <sub>2</sub> O ↔ CO <sub>2</sub> + H <sub>2</sub>	8.84E13	21.88	-0.3

$$k_{f,1} = A_1 T^{B_1} e^{-\frac{E_{a1}}{RT}} [CH_4]^{0.4} [O_2]^{1.4} \quad (R1)$$

$$k_{f,2} = A_2 T^{B_2} e^{-\frac{E_{a2}}{RT}} [H_2]^{0.7} [O_2]^{0.9} \quad (R2)$$

$$k_{f,3} = A_3 T^{B_3} e^{-\frac{E_{a3}}{RT}} [CO]^1 [O_2]^{0.5} \quad (R3)$$

$$k_{f,4} = A_4 T^{B_4} e^{-\frac{E_{a4}}{RT}} [CO]^1 [H_2O]^1 \quad (R4)$$

The optimization of the four-step mechanism is made, as schematically represented in Fig. 6, by matching the laminar burning velocity, fully burned values of the major emissions and adiabatic temperatures to predictions of the detailed GRI-Mech 3.0 reaction mechanism [49]. These are obtained by coupling the multi-objective optimization software ModeFrontier [50] with the CHEMKIN [51] software. The method consists of coupling the solving of given laminar premixed flames with an optimization procedure that dynamically adjusts the Arrhenius coefficients to match a set of reference laminar flames computed with

the fully detailed kinetics. Numerical simulations of all the reaction systems were conducted using CHEMKIN [51].

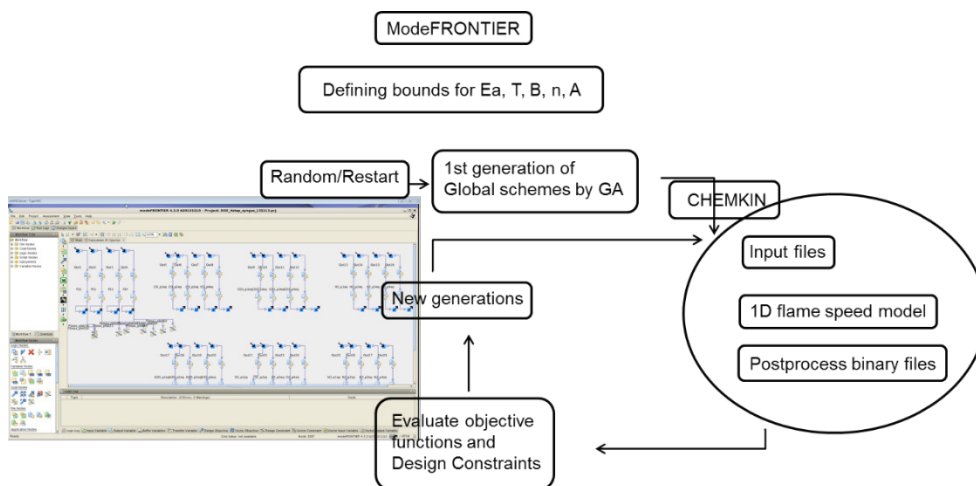


Figure 6. Layout of the chemical mechanism optimization [20].

The reference set is composed of 20 laminar premixed flames, decomposed into 5×4 flames distributed over equivalence ratios within the range of 0.5 - 1.0, inlet temperatures of 300 K – 800 K and methane–hydrogen mixtures with 0, 20, 40 and 60% hydrogen.

The optimization is first based on calculating the laminar burning velocity, the concentrations of the major species and the adiabatic flame temperature for the 20 laminar premixed flames using the detailed mechanism GRI-Mech 3.0 [49]. The solutions are stored as a reference target. Then, the optimization process starts randomly, based on the evaluation strategy algorithm [52], to adjust all pre-exponential factors, activation energies and temperature exponents,  $A$ ,  $E_a$  and  $n$  in Eq. (3). The new flame conditions are simulated with the laminar burning velocity equations and the sum of squared individual errors between the global mechanism and the detailed chemistry solutions are measured over target optimization points distributed among the reference flames. The objective function consists of the sum of the errors between the global and the detailed mechanism in terms of laminar burning velocities, adiabatic flame temperature and major species concentrations. A new set of parameters are determined to minimize the objective function. The process is then repeated; i.e. new flames are computed with the four-step reaction mechanism up to convergence. In the present work 2864 parameter conditions have been systematically simulated, Fig 7.

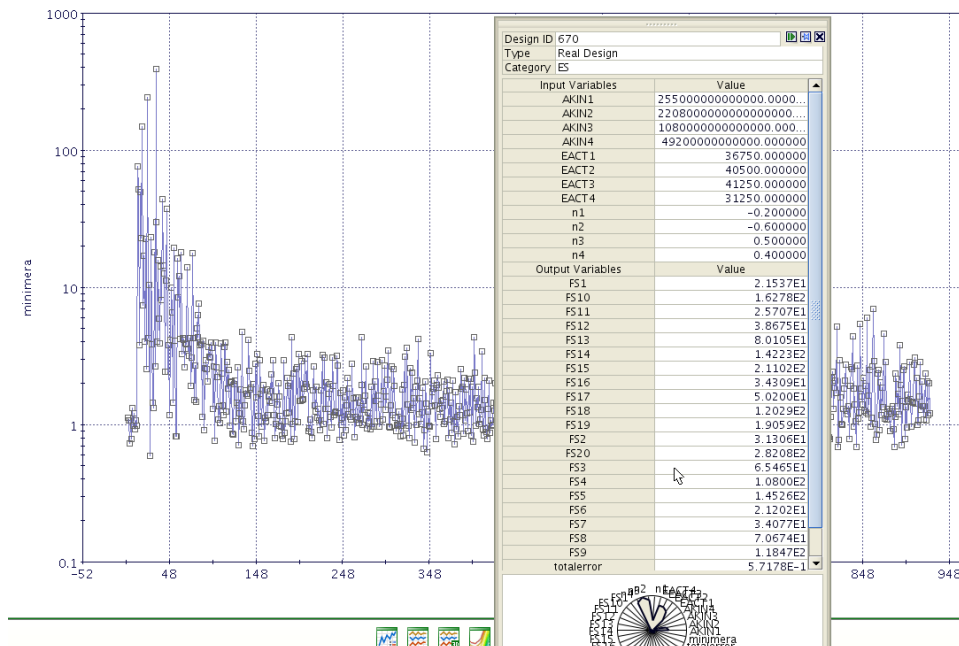


Figure 7. The sum of individual errors vs. design ID.

### 3.4 CFD OF LAMINAR FLAMES

#### 3.4.1 Method

Steady-state laminar flow simulations are performed to predict flow field and combustion characteristics. The combustion was modeled by finite-rate chemistry using species transport. The stiff chemistry solver was used together with thermal diffusion. The CFD model is shown in Fig. 8. The CFD simulations are made using Ansys Fluent V17 [53]. The CFD simulations were started from a non-reacting case and ignited by increasing the wall temperature in the nozzle. The total simulation time used for the three different reaction mechanisms GRI-Mech 3.0, Z42 and 4-step, using 128 nodes at the cluster, was 98, 40 and 8 hours, respectively.



Figure 8. The geometry for the burner setup, used in the CFD model.

The selected mesh is a fine multi-block structured mesh containing around 3.5 million hexahedral cells. Figure 9 shows selected surfaces of the structured grid of the single circular nozzle laboratory burner geometry. The commercial software ICEM CFD [53] is used for meshing. The grid is refined in the region around the flame to capture the wide range of scales present in the flow. The circular nozzle is visible in Fig. 9.

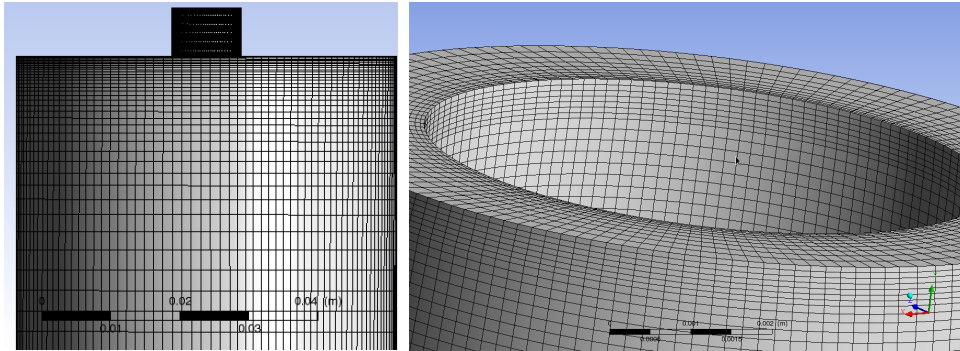


Figure 9. The hexahedral mesh in the burner where the nozzle is visible in the center.

### 3.4.2 Boundary conditions and evaluation planes

Specified velocities are set at the five inlet boundaries (marked #1 and #2 in Fig. 8) for the co-flow air (0.25 m/s) and the premixed fuel-air inlet (1.4 m/s). The total temperature is set to 298 K at the inlets. The outlet boundary condition (marked #3 in Fig. 8) is set to 1 atmosphere and all the walls are set to no-slip adiabatic walls. The total equivalence ratio in the burner is set to 1.

Figure 10 shows the six line locations along x-axis and the centerline, at which the CFD data were obtained. These lines are used to extract temperatures, velocities and species mass fractions. Five lines are denoted by locations 1 to 6 with increasing distance from the burner opening.

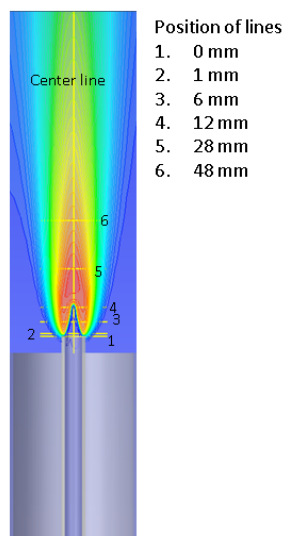


Figure 10. CFD simulation evaluation line locations marked with 1 to 6.

## 4 Laminar flames: Results and discussion

The results section starts with brief results from 1D flame simulations, identifying the expected trends in flame composition based on an established, detailed, kinetic mechanism. This is followed by validation of the developed global mechanism, first in 1D cases, then for CFD simulations of the laboratory flame. Finally, experimental results are presented and discussed in connection to relevant modeling results.

### 4.1 DETAILED KINETIC SIMULATIONS OF 1D FLAMES

Detailed kinetic modeling of planar 1D flames is an idealized case that in the present context is useful to investigate trends in reactivity and the underlying kinetics. The Bunsen type flames studied experimentally and using CFD in the present work are expected to show the same general trends regarding flame composition as the planar 1D flames, while the absolute numbers are not strictly comparable. In the following we point at some important trends in reactivity, and the understanding gained from this is later put in the context of the experimental study. The focus here is on concentrations of mainly CO and CH<sub>2</sub>O, while data is also available for a range of other species, including radicals.

The present study is focused on trends in reactivity as a result of difference in hydrocarbon mixture composition, pressure and amount of hydrogen addition. As was concluded by Nilsson et al. [7], for atmospheric pressure flames the different hydrocarbon mixtures are affected differently by hydrogen addition. The slowest burning fuel, pure methane, show larger enhancement effects compared with the mixtures containing ethane and propane. This is the result of increased radical production, in particular for H atoms. In Fig. 11 it is shown how concentrations of formaldehyde and CO vary with equivalence ratio for different amounts of hydrogen addition. 10% hydrogen makes essentially no difference at all whereas the difference between 60% and 80% is quite significant; the chemistry goes from a significantly hydrocarbon dominated state to one where hydrogen is starting to play a significant role.

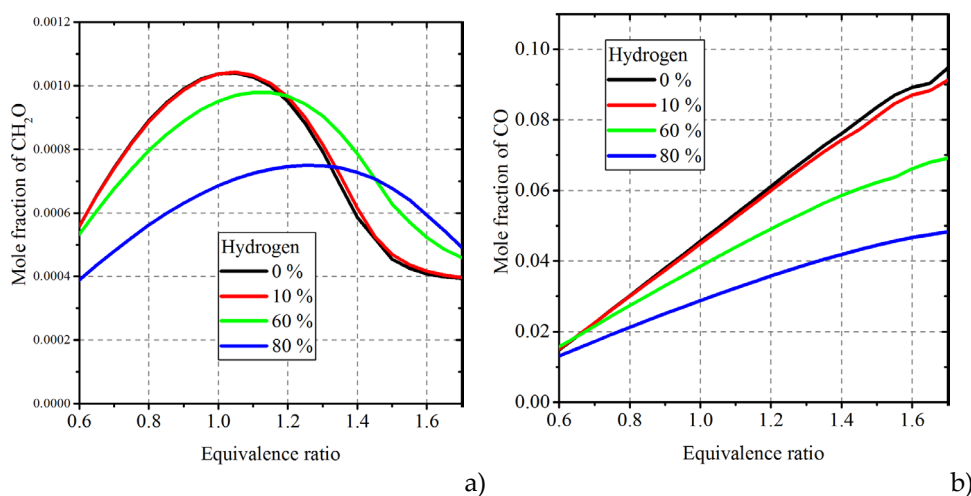


Figure 11. Mole fractions of a) formaldehyde, and b) carbon monoxide, for laminar flames of methane at 298 K and 1 atm., with various amount of hydrogen addition.

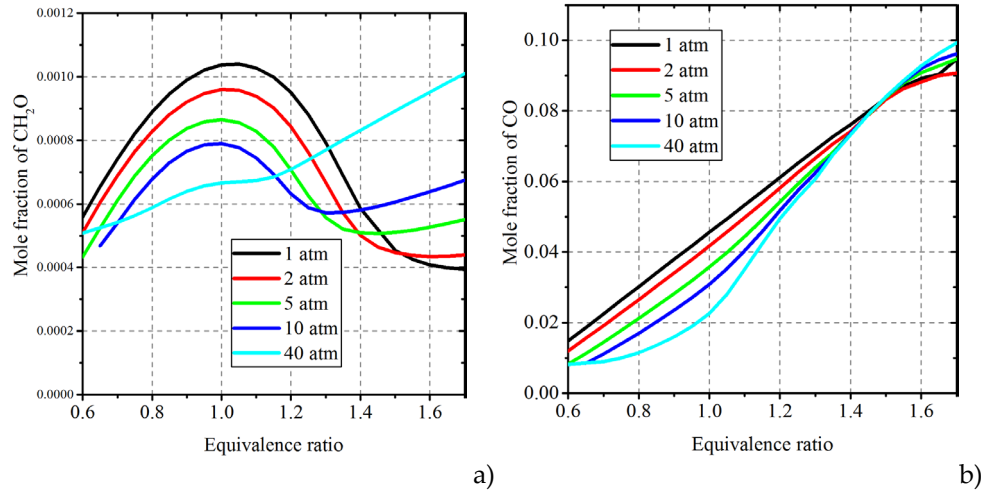


Figure 12. Mole fractions of a) formaldehyde, and b) carbon monoxide, for laminar flames of methane at 298 K and 1 atm., at various pressures.

Figure 12 shows the trends in  $\text{CH}_2\text{O}$  and CO concentration versus equivalence ratio for a methane/air flame at different pressures. Just like in the case of hydrogen addition the effects are significantly different at lean and rich conditions.

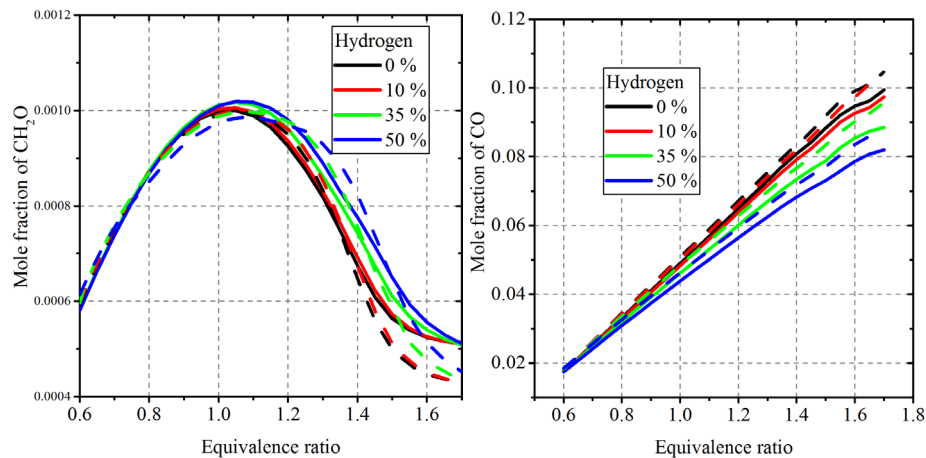


Figure 13. Mole fractions of a) formaldehyde, and b) carbon monoxide, for laminar flames of methane/ethane (full drawn lines) and methane/propane (dashed lines) at 298 K and 1 atm., for several hydrogen fractions.

Figure 13 presents formaldehyde and CO concentrations for two of the hydrocarbon blends, at various hydrogen concentrations within the hydrocarbon dominated regime. At lean conditions the concentrations are similar, independent on hydrocarbon or hydrogen composition, while at rich conditions CO concentration decreases, and more so for the methane/ethane flame.

## 4.2 PERFORMANCE OF A GLOBAL MECHANISM

In this section development of a 4-step mechanism suitable for CFD simulations of turbulent combustion is described and compared with more complex mechanisms

using simulations of 1D flames. Figures showing important results are presented in the following, while additional validation is provided in Appendix B.

Figures 14 and 15 show the numerically calculated results from laminar burning velocities and adiabatic flame temperature using different methane-hydrogen-air mixtures at different inlet temperatures and equivalence ratios obtained with the detailed reaction mechanism GRI-Mech 3.0 [49], reaction mechanism Z42 [17] and the present optimized global mechanism consisting of four reactions. Lean conditions and high inlet temperatures are chosen since this is representative for the gas turbine combustors the mechanism eventually will be used to simulate. The four-step global reaction mechanism shows good agreement at the lean conditions at all inlet temperatures and mixtures. Some discrepancy is visible towards the stoichiometric condition for the mixture 40% CH<sub>4</sub>, 60% H<sub>2</sub> at inlet temperature 295 K. The global mechanism at this condition under predicts the laminar burning velocity by 15%. Summarizing the total error at all conditions analyzed shows that the laminar burning velocity is over predicted by 0.8%, which is quite small compared to common experimental uncertainties for S<sub>L</sub>. The results also as expected show that an increased fraction of hydrogen corresponds to an increase in laminar burning velocity. The rich side was not included in the optimization due to simplification. Previous experience shows that the rich side is more difficult to match between the detailed and the reduced mechanisms and some type of correction function is needed, see e.g. ref. [1, 2].

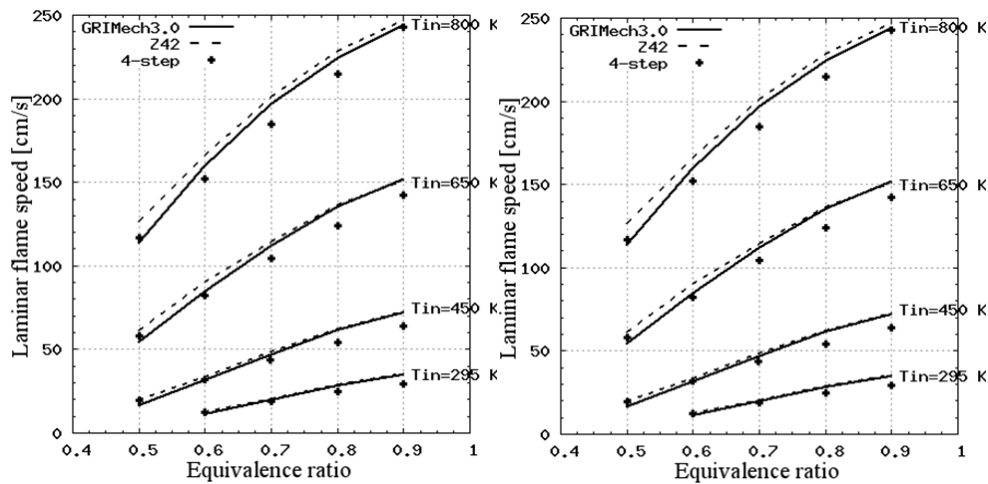


Figure 14. Burning velocity versus equivalence ratio,  $p=1\text{atm}$ . Left: 100% CH<sub>4</sub>, Right: 60% CH<sub>4</sub>, 40% H<sub>2</sub>.

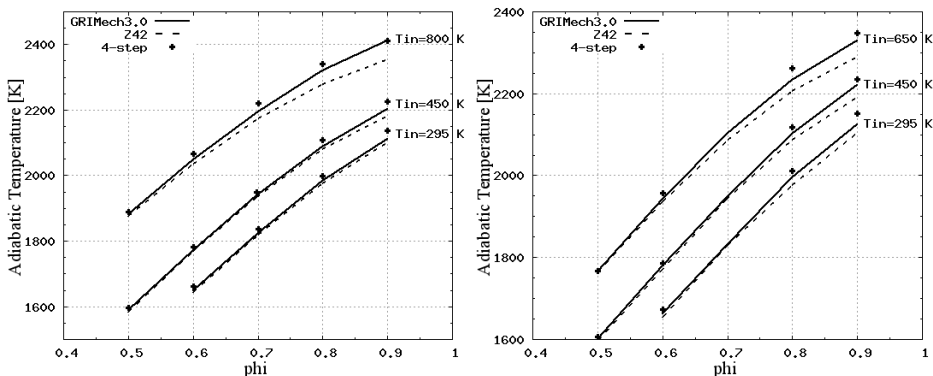


Figure 15. Adiabatic flame temperature vs. equivalence ratio,  $p=1\text{atm}$ . Left: 100%  $\text{CH}_4$ . Right: 60%  $\text{CH}_4$ , 40%  $\text{H}_2$ .

Figures 16-17 show  $\text{CO}_2$  and  $\text{H}_2\text{O}$  mole fractions using different methane-hydrogen air mixtures at different inlet temperatures and equivalence ratios, calculated with the detailed reaction mechanism GRI-Mech 3.0, reaction mechanism Z42 and the present optimized global mechanism consisting of four reactions. The four-step global reaction mechanism predicts the above species well at all inlet temperatures and mixtures.

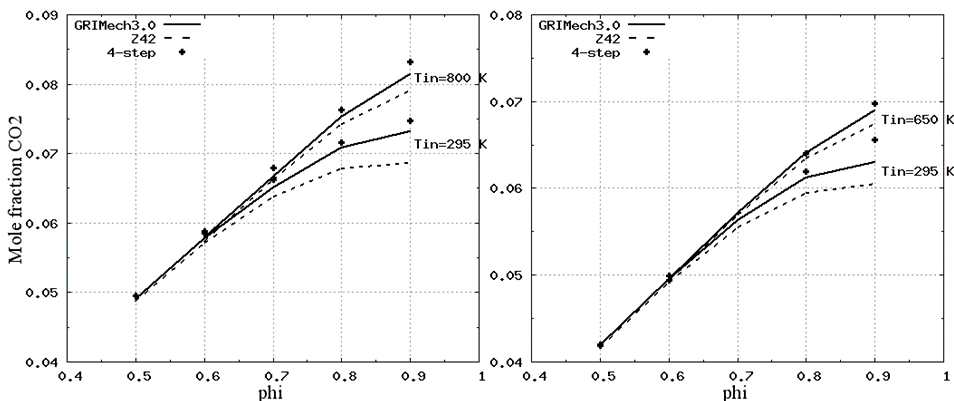


Figure 16.  $\text{CO}_2$  mole fraction vs. equivalence ratio, Left: 100%  $\text{CH}_4$ , Right: 60%  $\text{CH}_4$ , 40%  $\text{H}_2$ .

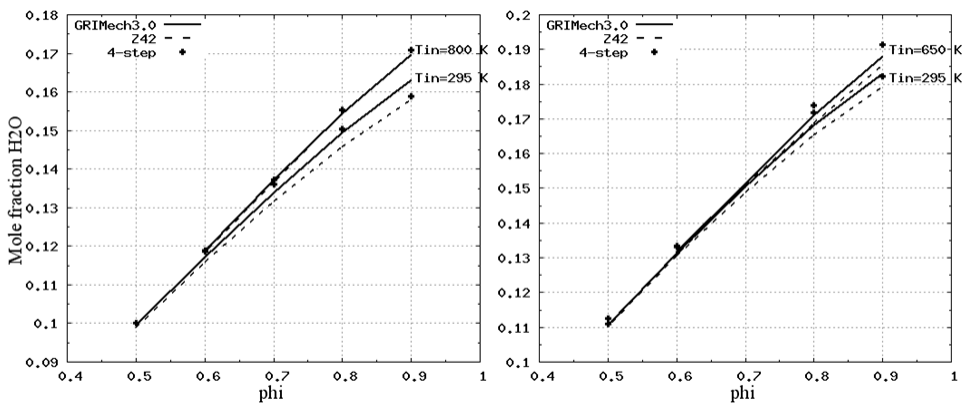


Figure 17.  $\text{H}_2\text{O}$  mole fraction vs. equivalence ratio, Left: 100%  $\text{CH}_4$ , Right: 60%  $\text{CH}_4$ .

## 4.3 CFD SIMULATIONS METHANE/AIR FLAMES

### 4.3.1 Contour plots

In this section the three mechanisms at different level of complexity are used in CFD simulations of a laminar flame. The aim is to compare the results to enable evaluation of the performance in relation to the computational time. Characteristics of the mechanisms, GRI-Mech 3.0, Z42 and global 4-step, are given in Table 2. Results of importance to the discussion are included as figures in the following text, while additional figures of temperatures, axial velocities and species profiles are available in Appendix C.

Figure 18 shows contour plots of the temperature [K] for combustion of 100% CH<sub>4</sub> at stoichiometry using mechanisms GRI-Mech 3.0, Z42 and the 4-step optimized mechanism. All mechanism in general shows a similar level of temperature prediction. The unburnt fuel and air in the center of the tube has room temperature. Above this region the conical V-flame is located at the top of the fuel nozzle. Small differences can be observed around the region of intense combustion (the reaction zone). The four-step mechanism shows a thinner reaction zone while the detailed GRI-Mech 3.0 shows a reaction zone that is more curved than the other two mechanisms. The post-flame zone which is located above the conical V-shape flame is very similar for all three cases.

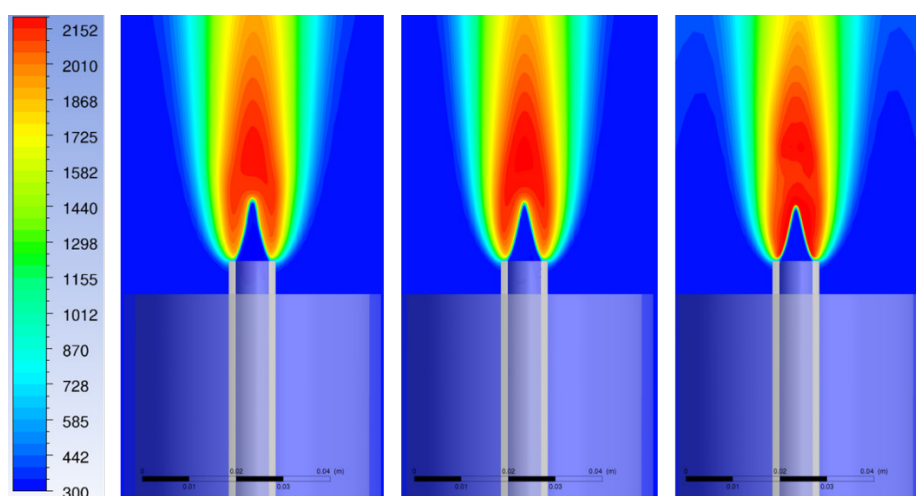


Figure 18. Temperature [K] for 100% CH<sub>4</sub>. Left: GRI-Mech 3.0, middle: Z42, right: four-step

Figure 19 shows contour plots of the CO mass fraction for combustion of 100% CH<sub>4</sub> at stoichiometry using the mechanisms GRI-Mech 3.0, Z42 and the present optimized mechanism. The steady-state laminar flame simulations with mechanisms GRI-Mech 3.0 and Z42 show fairly similar levels of CO prediction. However, the present four-step mechanism under-predicts the CO level while the flame shape and flame position are correctly predicted.

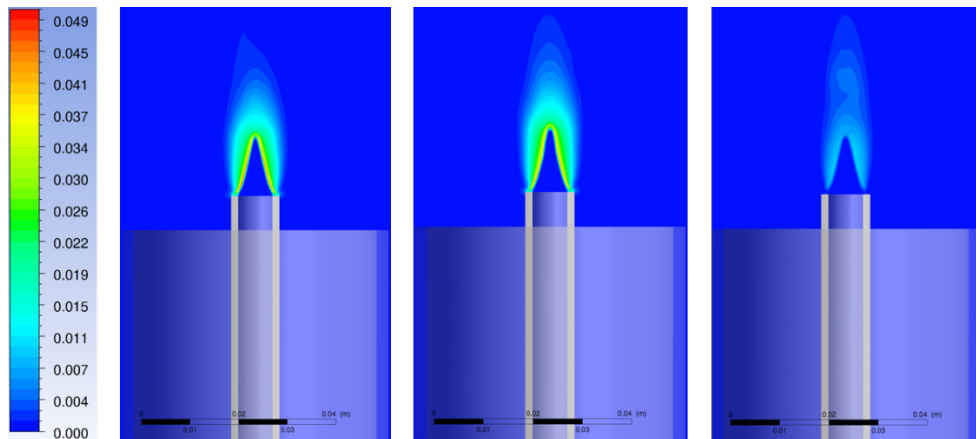


Figure 19. CO mass fraction for 100% CH<sub>4</sub>. Left: GRI-Mech 3.0, middle: Z42, right: four-step

Figure 20 shows contour plots of the OH mass fraction for combustion of 100% CH<sub>4</sub> at stoichiometry using mechanisms GRI-Mech 3.0 and Z42. The present optimized mechanism is not included in the figure since the OH-species is not included in the mechanism. The steady-state laminar flame simulations with mechanisms GRI-Mech 3.0 and Z42 show fairly similar flame shape and flame position. However, in the plot it is visible that the Z42 mechanism predicts higher OH mass fraction around the reaction zone.

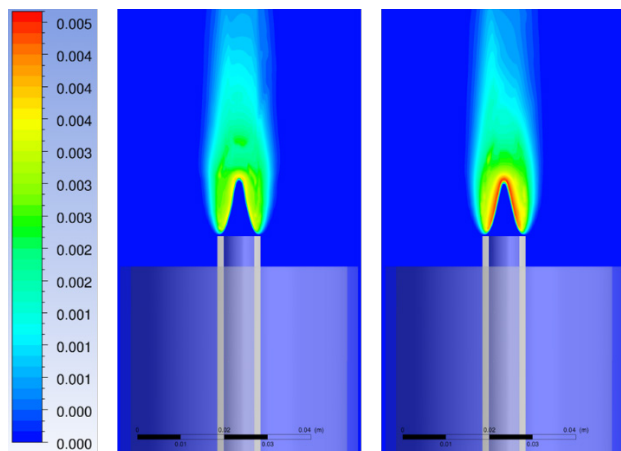


Figure 20. OH mass fraction for 100% CH<sub>4</sub>. Left: GRI-Mech 3.0, right: Z42

#### 4.3.2 Temperature and velocity profiles

Predictions of radial static temperature profiles for combustion of the methane-air mixture at stoichiometric condition, at a position close to the burner outlet and at some distance up in the flame cone, using the three mechanisms, are presented in Fig. 21a. At the lower position the agreement between mechanisms is excellent, while at the higher position the simplest mechanism over predicts the temperature with about 200 K. Figure 21b presents profiles at various positions in the flame from the most detailed mechanism, GRI-Mech 3.0. Axial velocities in x- and y-directions are compared in Fig. 20. Small differences can be seen between the mechanisms, most notably the 4-step global reaction mechanism over predicts the

axial velocity by 10 % at 1 mm above the burner orifice (at radial coordinate = 0.005m). This is correlated to the over predicted temperature at the corresponding location.

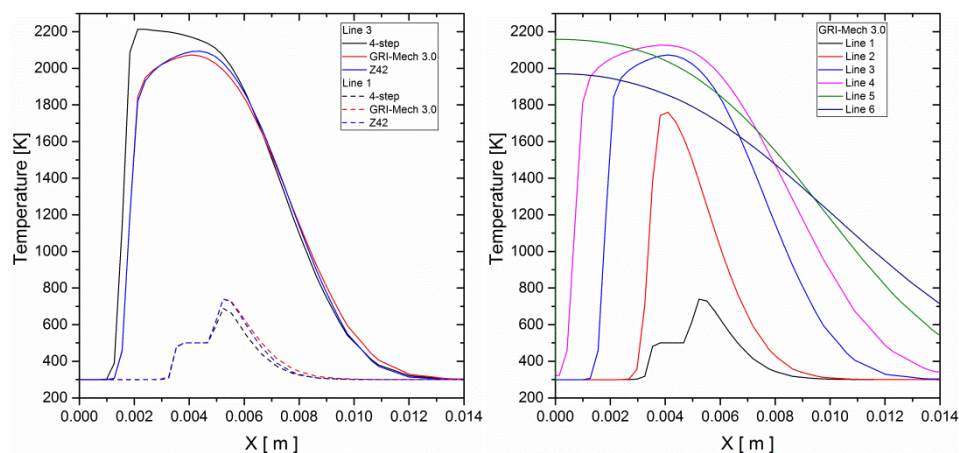


Figure 21. Static temperature for flame with 100% CH<sub>4</sub>. a) Lines 1 and 3 for all three mechanisms, b) all lines for GRI-Mech 3.0.

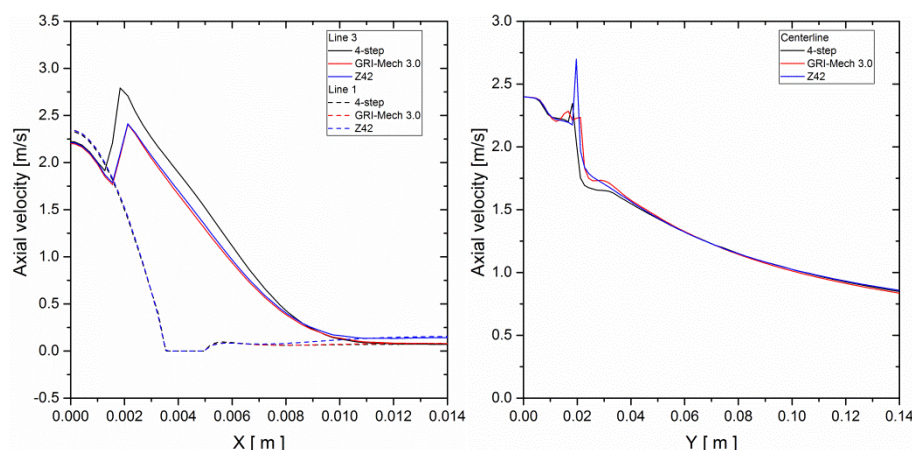


Figure 22. Axial velocity for flame with 100% CH<sub>4</sub>. a) at two distances from the burner, b) along the centerline.

### 4.3.3 Species concentration profiles

Figure 23 presents species profiles, CH<sub>4</sub>, O<sub>2</sub>, H<sub>2</sub>O, CO, H<sub>2</sub> and CO<sub>2</sub> along the centerline of the methane/air flame at equivalence ratio 1, for all three mechanisms. Results are very similar for the three mechanisms, except that the 4-step mechanism shows sharper profiles around the reaction zone, Y=0.02 m, in line with the narrow reaction zone seen in Fig. 19c. This is a common behavior of a highly simplified mechanism since the chemistry occurs in fewer steps than in the more detailed, realistic, case. The results, along with other simulations, show that both the Z42 and the present 4-step mechanism adequately predict species concentrations in comparison with the more detailed GRI-Mech 3.0, at stoichiometric condition. Thereby, they would also yield a satisfactory prediction of the heat release. The 4-step mechanism tends to overpredict the CO<sub>2</sub> concentration at distance 6-12 mm from the burner orifice related to the

overprediction in temperature at the same position. This may be due to the insufficiently accurate resolution of the flame.

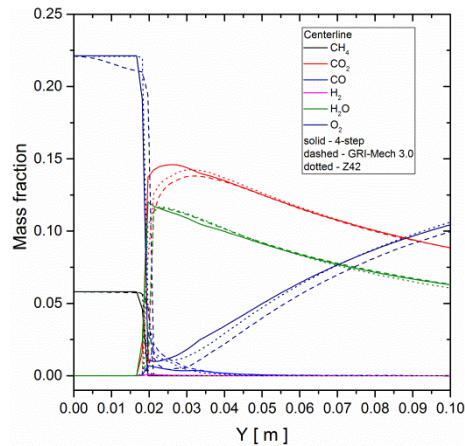


Figure 23. Mass fraction of important species at center-line, 100% CH<sub>4</sub>.

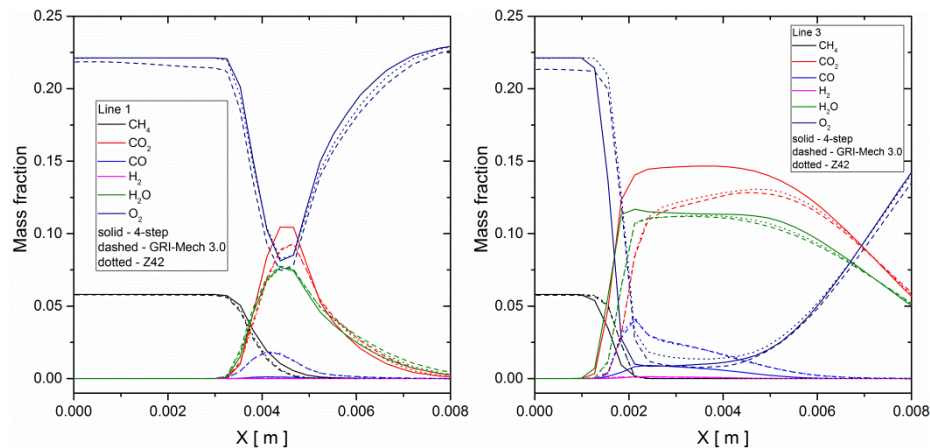


Figure 24. Mass fraction of important species at lines 1 and 3, 100% CH<sub>4</sub>.

Figure 24 presents species profiles in the radial direction close to the burner exit (24a) and further up in the flame cone (24b). The agreement between the three mechanisms is excellent at the lower position, while at the higher position the 4-step mechanism shows a significantly narrower reaction zone, i.e. the species profiles are steeper. A significant difference is also that the 4-step mechanism under predicts CO and has a corresponding over prediction of CO<sub>2</sub>, which means that the reaction proceeds too fast and thus result in the higher temperature seen in Fig. 21a.

Regarding CO profiles, both the 4-step and the Z42 mechanism predicts the position of the peak CO concentrations correct radially and axially. However, the 4-step mechanism fails to predict the peak value of the CO concentration at all positions and may not be sufficiently accurate for CO emission modeling. This can be explained from the fact that the CO concentration was not included in the objective function in the optimization of the 4-step mechanism. However, if it had been included in the optimization, it is not certain that the prediction of CO would

have been accurate since no radicals are included in the global reaction mechanism.

#### 4.4 CFD SIMULATIONS: VARIATION OF H<sub>2</sub> CONCENTRATION

Figure 25 shows contour plots of the OH mass fraction for various amounts of hydrogen added to methane/air mixture at stoichiometry using the mechanism Z42 and Fig. 26 shows the corresponding temperature plot for the same cases. For the steady-state laminar flame simulations hydrogen addition considerably alters the global flame characteristics by different flame shapes and flame positions. As shown, an increased amount of hydrogen implies a shorter and smaller flame. This behavior is in line with expectations since an increased amount of hydrogen implies an increased burning velocity. Since the flow velocity is kept constant in the CFD simulations, the increased burning velocity means that the flame moves closer to the nozzle and finally into the nozzle for the highest hydrogen content. The flame is also clearly more unstable at higher hydrogen addition.

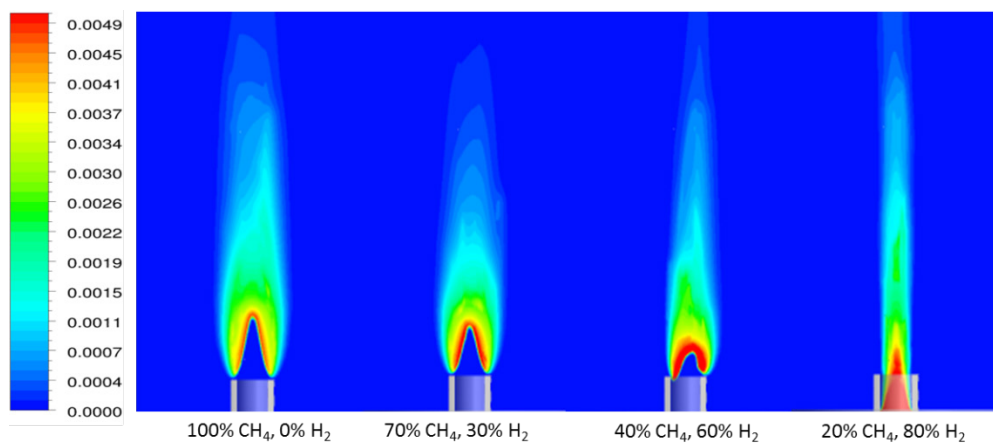


Figure 25. OH mass fraction for simulations of stoichiometric flames using the Z42 mechanism for different fuel mixtures.

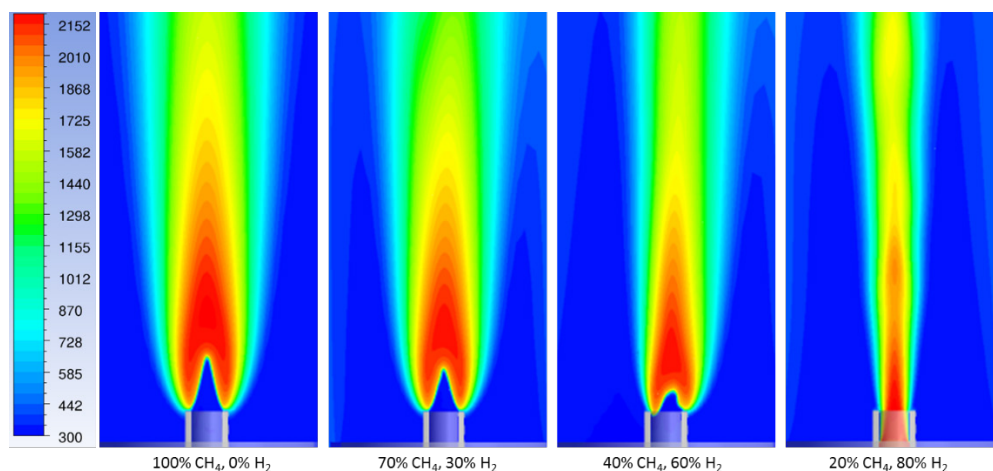


Figure 26. Temperature [K] for simulations of stoichiometric flames using the Z42 mechanism for different fuel mixtures.

## 4.5 EXPERIMENTAL RESULTS

### 4.5.1 Laminar burning velocity

Figure 27 shows sample photos of investigated Bunsen-type flames in the high-pressure burner.

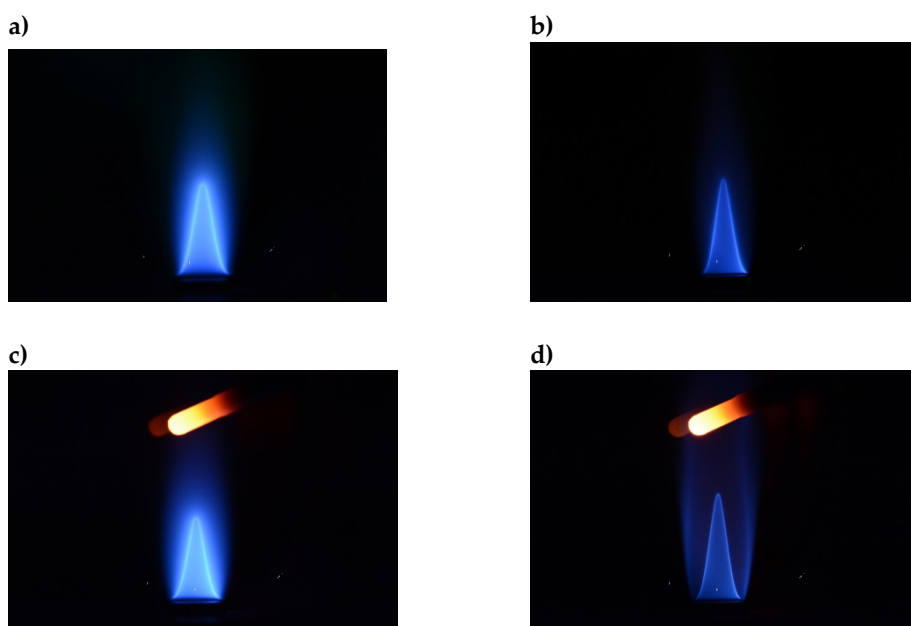
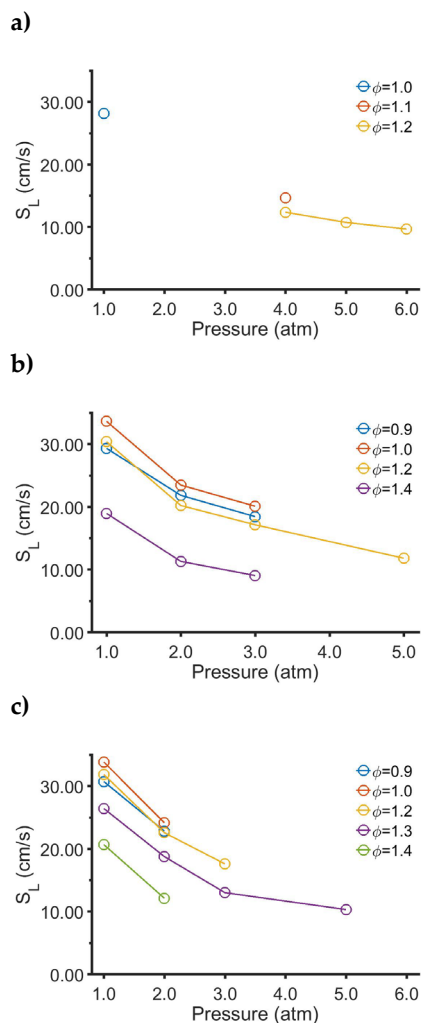


Figure 27. Photos of premixed flames stabilized on the burner of the high-pressure vessel. a) CH<sub>4</sub>-air flame  $\Phi=1.0$ ,  $p=1$  atm., b) CH<sub>4</sub>-air flame  $\Phi=1.2$ ,  $p=6$  atm. c) CH<sub>4</sub>(65%)-H<sub>2</sub>(35%)-air flame  $\Phi=1.0$ ,  $p=1$  atm., d) CH<sub>4</sub>(65%)-H<sub>2</sub>(35%)-air flame  $\Phi=1.3$ ,  $p=5$  atm. All flames show blue chemiluminescence from excited radical species and flame reaction zone is indicated by a thin blue cone. For the flames supplied with hydrogen (c and d) the temperature of the hot combustion products have made the ceramic ignition rod, positioned above the flame, glow orange-yellow.

All flames feature a conical shape and the flows were adapted in order to achieve similar flame heights for different fuels, equivalence ratios and pressures. This approach was made to ensure that the laser beam for Raman spectroscopy measurements, propagating across the flame cone, passed through flame regions of similar size for the different measurements. Thus, the investigated flames look similar in the photos and all feature a blue-green luminescence generated from excited radical species such as CH and C<sub>2</sub>, created in the chemical reactions. In particular, the flame reaction zone can be distinguished by the chemiluminescence from excited CH radicals and is visible as thin bright blue cone in the photos of Fig. 27.

Photos such as those presented in Fig. 27 can be employed for estimation of the laminar burning velocity,  $S_L$ , according to the approach presented in section 2.5 and Fig. 28 presents values of  $S_L$  for flames burning the following fuels or fuel mixtures  $\text{CH}_4$ ,  $\text{CH}_4(75\%)\text{-H}_2(25\%)$ , and  $\text{CH}_4(65\%)\text{-H}_2(35\%)$  at different equivalence ratios and pressures.



**Figure 28.** Laminar burning velocities for flames of  $\text{CH}_4$  (a),  $\text{CH}_4$  75%  $\text{H}_2$  25% (b), and  $\text{CH}_4$  65%  $\text{H}_2$  35% (c) versus pressure at different equivalence ratios ( $\Phi$ ).

For a stoichiometric  $\text{CH}_4$ -air flame at atmospheric pressure, as displayed in Fig. 27a, evaluation gives  $S_L=28$  cm/s. More accurate measurements of  $S_L$  at atmospheric pressure using a flat flame in a special so-called heat-flux burner configuration, result in a value of  $S_L=36$  cm/s [7]. Thus, the value obtained for the conical flame in the high-pressure burner is underestimated by 22%. However, the evaluation is based on the gas flow speed of the unburned gas mixture set at room temperature, and preheating of the unburned gas in the burner, indicated by temperature measurements using Raman spectroscopy, would increase the value and bring it closer to that obtained by the heat-flux method. As mentioned in the methodology section, the main aim of the present study is not the absolute determination of laminar burning velocities, but the comparison of changes between results obtained at different conditions.

The burning velocity decreases with equivalence ratio as well as with increasing pressure (cf. Fig. 28a) and for a fuel-rich flame of  $\Phi=1.2$  at a pressure of 6 atm. the evaluated burning velocity is  $S_L=10$  cm/s.

Replacing part of the  $\text{CH}_4$  with  $\text{H}_2$  in the fuel mixture enhances the burning velocity, as reported previously (cf. Fig. 1). At atmospheric pressure and stoichiometric combustion ( $\Phi=1.0$ ) the laminar burning velocity for fuel mixtures  $\text{CH}_4(75\%)-\text{H}_2(25\%)$  and  $\text{CH}_4(65\%)-\text{H}_2(35\%)$  is 34 cm/s. Thus, both mixtures result in an 21% enhancement of the burning velocity. Previous investigations of flat atmospheric-pressure flames at equivalence ratio  $\Phi=1.0$  (cf. Fig. 1) show an increase from  $S_L=36$  cm/s to  $S_L=45$  cm/s and  $S_L=47$  cm/s for addition of 25% and 35%  $\text{H}_2$ , respectively. The relative increase of 25% and 30% for these two cases is fairly consistent with the 21% increase obtained for the conical flames. At a pressure of 5 atm. the burning velocity is  $S_L=12$  cm/s for addition of 25%  $\text{H}_2$  and  $S_L=10$  cm/s for 35%  $\text{H}_2$ , respectively. Compared with the value of  $S_L=11$  cm/s for the pure  $\text{CH}_4$  flame at  $\Phi=1.2$  and 5 atm., the differences are small, suggesting that combustion enhancement by hydrogen addition is suppressed at fuel-rich conditions and elevated pressure.

#### 4.5.2 Species concentration profiles: Hydrocarbon combustion

Figure 29 presents radial species concentration profiles measured by Raman spectroscopy in  $\text{CH}_4$ -air flames.

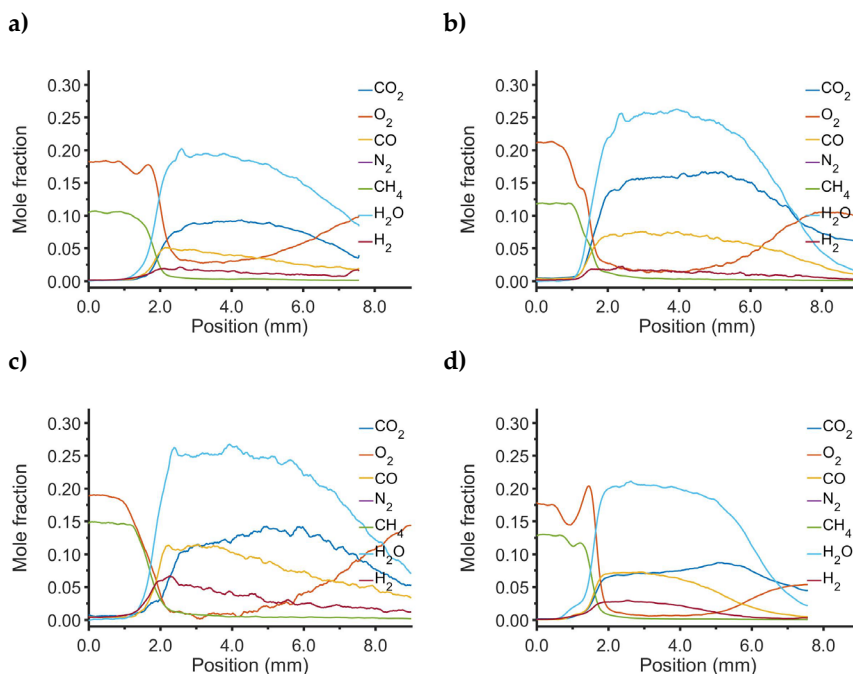


Figure 29. Radial species concentration profiles in  $\text{CH}_4$ -air flames a)  $\Phi=1.0$ ,  $p=1$  atm., b)  $\Phi=1.0$ ,  $p=3$  atm., c)  $\Phi=1.3$ ,  $p=1$  atm., d)  $\Phi=1.2$ ,  $p=6$  atm.,

Profiles for an atmospheric-pressure flame of  $\Phi = 1.0$  are shown in Fig. 29a, starting from the unburned mixture at position 0 mm in the flame center fuel and oxygen concentrations are at their initial concentrations values set by the experimental conditions. At position  $\sim 1.5$  mm both fuel and oxygen profiles show a sharp

decreasing gradient as they enter the flame front region where chemical reactions are initiated and advance. Simultaneously, the concentrations of major products  $\text{CO}_2$  and  $\text{H}_2\text{O}$  start to increase and reach their final values at position  $>2$  mm, further on at positions  $>5$  mm these species concentrations start to decrease due to mixing with the atmosphere surrounding the flame in the burner vessel. This is also seen by an increase in the oxygen level at positions beyond 6 mm. The combustion products also include  $\text{CO}$  and  $\text{H}_2$  reaching peak levels in the vicinity of the flame front region and gradually decreasing with radial distance from the flame front. The carbon monoxide concentration reaches a value of around 5%, in good agreement with model predictions presented in Fig. 12b and 24b. A stoichiometric flame at elevated pressure of 3 atm. shows similar profiles, as presented in Fig. 29b. While modeling predicts a slight decrease in  $\text{CO}$  formation with elevated pressure (cf. Fig. 12b) the experimental  $\text{CO}$  concentrations are similar for the atmospheric flame and the 3 atm. flame. However, the experimental concentrations are dependent on the actual temperature of the flame as well as the time required to obtained full  $\text{CO}$  oxidation, determined by the burning velocity.

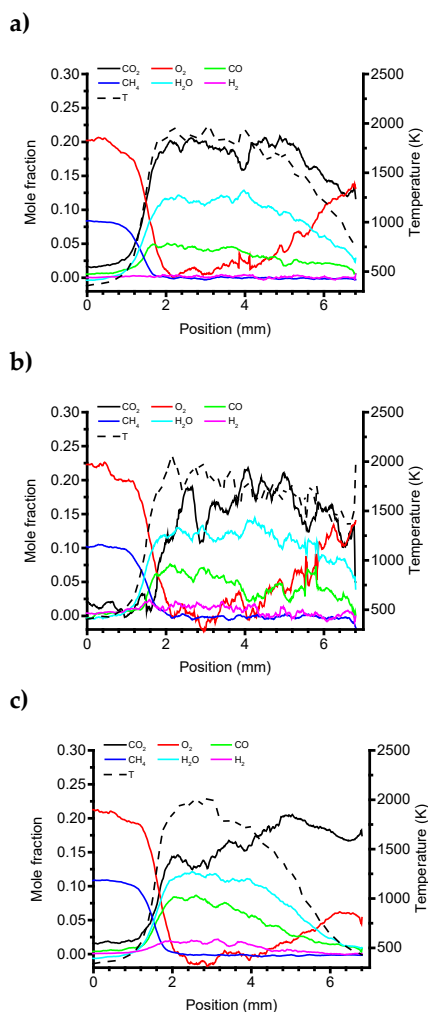


Figure 30. Radial species concentration profiles in  $\text{CH}_4(80\%)\text{-C}_2\text{H}_6(20\%)\text{-air}$  flames a)  $\Phi=1.0$ ,  $p=3$  atm., b)  $\Phi=1.3$ ,  $p=1$  atm., c)  $\Phi=1.3$ ,  $p=8$  atm.

Fuel-rich combustion results in higher amounts of CO and H<sub>2</sub>, as evident from the profiles measured in an atmospheric flame of  $\Phi=1.3$  presented in Fig. 29c. At elevated pressure of 6 atm., presented in Fig. 29d, CO concentrations are lower, in agreement with model predictions presented in Fig. 12b.

Figure 30 presents concentration and temperature profiles measured for flames burning a fuel mixture of CH<sub>4</sub> (80%) and C<sub>2</sub>H<sub>6</sub> (20%). Similar trends as for methane combustion is also observed for the hydrocarbon mixture flames.

#### 4.5.3 Species concentration profiles: Hydrogen addition

Figures 31 and 32 show concentration profiles measured in flames with fuel mixtures containing 25% and 35% of H<sub>2</sub>, respectively. The general profile trends and features are similar to those observed for the CH<sub>4</sub> flames presented in Fig. 29. With hydrogen added to the fuel the profiles also show H<sub>2</sub> in the region of unburned reactant species at positions <2 mm. For stoichiometric combustion of the CH<sub>4</sub>(75%)-H<sub>2</sub>(25%) mixture at pressures of 1 and 3 atm., presented in Fig. 31a-b, the species profiles for CH<sub>4</sub>, H<sub>2</sub>, O<sub>2</sub>, CO<sub>2</sub>, and H<sub>2</sub>O are similar, while a decrease in CO formation is observed for the higher pressure.

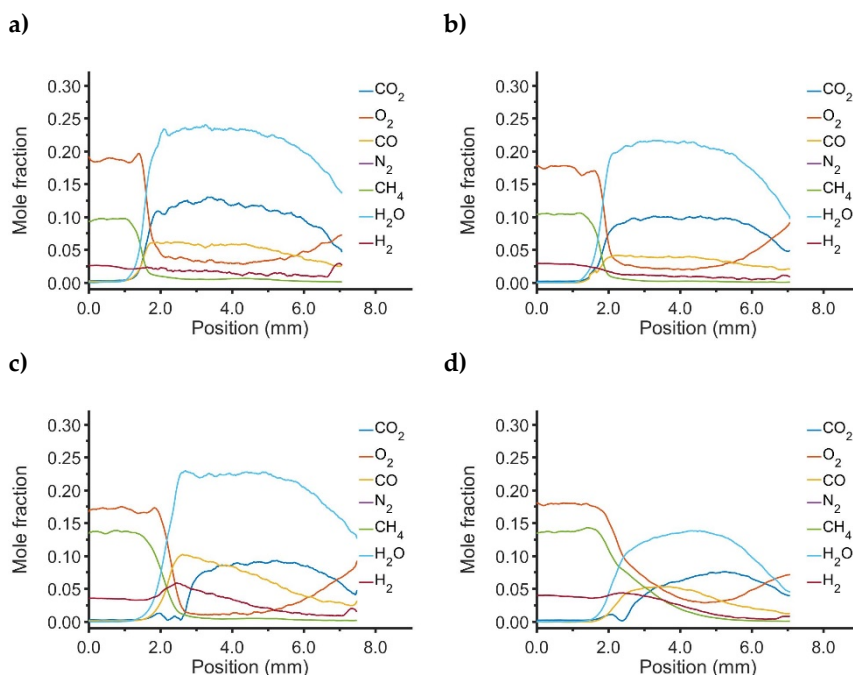
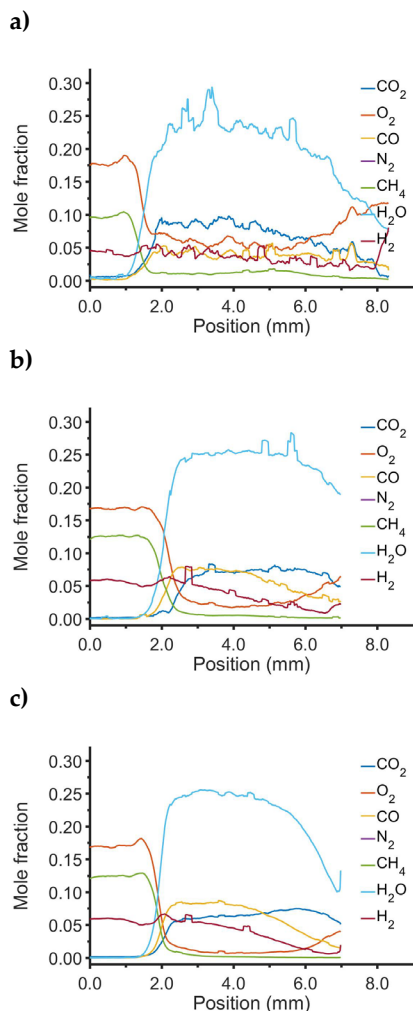


Figure 31. Radial species concentration profiles in CH<sub>4</sub>(75%)-H<sub>2</sub>(25%)-air flames a)  $\Phi=1.0$ ,  $p=1$  atm., b)  $\Phi=1.0$ ,  $p=3$  atm., c)  $\Phi=1.4$ ,  $p=1$  atm., d)  $\Phi=1.4$ ,  $p=3$  atm.

For fuel-rich combustion at  $\Phi=1.4$ , profiles displayed in Fig. 31c-d, CO and H<sub>2</sub> concentrations are higher than for the stoichiometric flames and a decrease in CO concentration with increase in pressure is also observed for the fuel-rich flames. The  $\Phi=1.4$  flame at pressure 3 atm. also shows a reduced H<sub>2</sub>O concentration level, potentially due to water condensation. Profiles for flames burning the CH<sub>4</sub>(65%)-H<sub>2</sub>(35%) fuel mixture are shown in Fig. 32 for stoichiometric (a) and fuel-rich (b) combustion at atmospheric pressure and fuel-rich combustion at 5 atm. pressure

(c). The hydrogen concentration measured in the unburned reactant mixture is as expected higher for these flames while other species show similar trends as observed for the CH<sub>4</sub>(75%)-H<sub>2</sub>(25%) mixture (cf. Fig. 31).



**Figure 32. Radial species concentration profiles in CH<sub>4</sub>(65%)-H<sub>2</sub>(35%)-air flames a)  $\Phi=1.0$ ,  $p=1$  atm, b)  $\Phi=1.3$ ,  $p=1$  atm, c)  $\Phi=1.3$ ,  $p=5$  atm.**

Figure 33 summarizes measured CO concentrations averaged over the flame product zone for flames of the CH<sub>4</sub>(75%)-H<sub>2</sub>(25%) and CH<sub>4</sub>(65%)-H<sub>2</sub>(35%) fuel mixtures.

Fuel-rich conditions at  $\Phi > 1$  produce higher amounts of CO with molar fractions of 4-5% for flames of both fuel mixtures. The experimental data show no significant difference between CO concentrations measured for the two fuel mixtures and modeling also predicts a rather limited influence on CO formation for these amounts of hydrogen (cf. Fig. 11b). For the lean ( $\Phi=0.9$ ) and stoichiometric conditions average CO levels are lower and the results indicate a decrease in CO formation with pressure, in agreement with modeling predictions (cf. Fig. 12b).

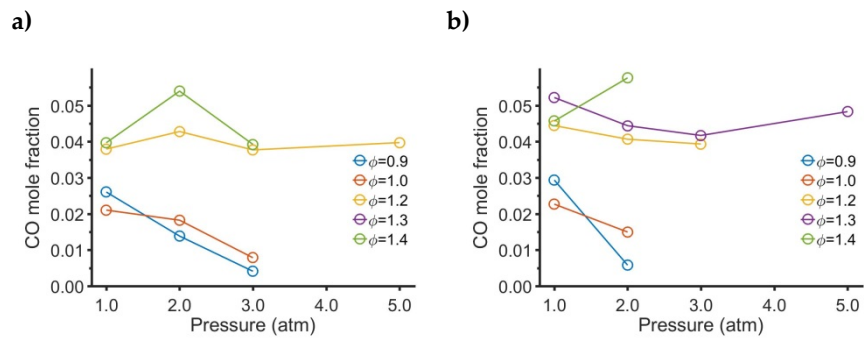


Figure 33. CO concentration for CH<sub>4</sub>-H<sub>2</sub> flames at different pressures and stoichiometries. a) CH<sub>4</sub> 75% H<sub>2</sub> 25%, b) CH<sub>4</sub> 65% H<sub>2</sub> 35%.

## 5 Simulation of industrial burner

In this section CFD predictions of a real gas turbine burner are presented. Two studies are carried out. One where the modelling strategy in the laminar flame section above is applied to a real gas turbine case using methane as fuel [54] and one where the influence of hydrogen addition is studied in an atmospheric combustion rig with full pre-heating [55]. The SGT-800 is a single-shaft gas turbine fitted with 30 Siemens 3<sup>rd</sup> generation DLE burners. The burners use swirl stabilization to maintain a stable combustion. For additional stability, twelve pilot flames are surrounding the main flame in each burner and the fuel distribution between the main and pilot flames can be adjusted during operation.

### 5.1 METHOD

The burner used is the Siemens SGT-800 fitted to the real engine combustion chamber or to an atmospheric combustion rig. The setup in the atmospheric rig is shown in Fig. 34.

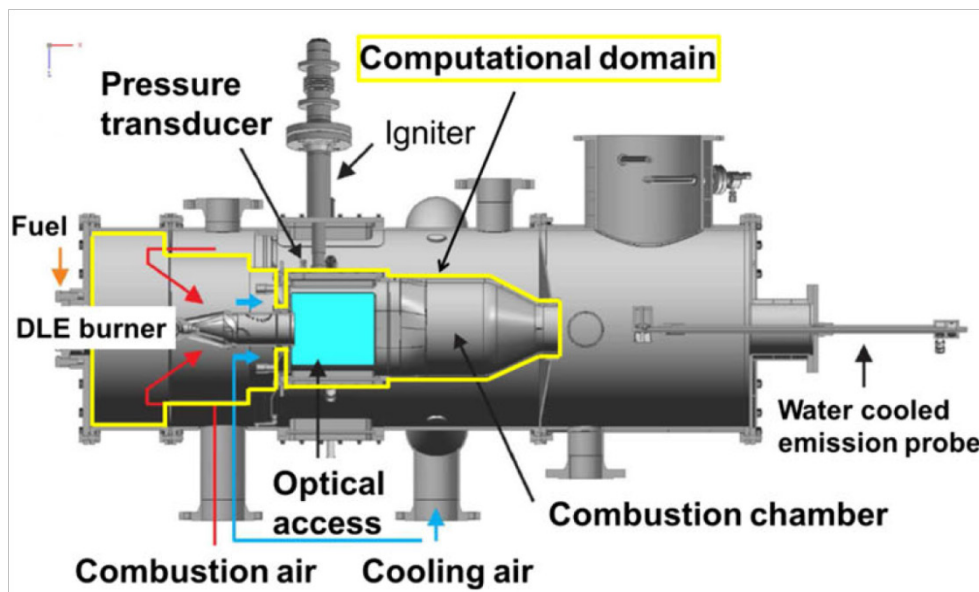


Figure 34. The SGT-800 burner fitted to an atmospheric combustion rig.

Scale-resolved turbulence modes are used in both cases to capture the dynamic behavior of a gas turbine flame. In the real engine case a pure methane flame is studied using the four-step chemical mechanism from the laminar flame section. In the atmospheric case both a pure methane flame and a 20% (by volume) methane and 80% hydrogen flame are studied. The chemistry is based on a flamelet assumption that the chemistry is affecting the turbulence but the local turbulence is not affecting the chemistry so that detailed chemistry may be used for tabulation. The tables are generated using GRI-Mech 3.0.

## 5.2 RESULTS AND DISCUSSION

### 5.2.1 Real engine case without hydrogen addition

The performance of the global chemical kinetics scheme is here compared against some engine data and against other types of combustion models. The model performs well with prediction of a stable flame at the expected location, cf. Fig. 35. The reaction progress in finite-rate-chemistry models is estimated using the fuel mass fraction relative to its value in both reactants and products. The flame is conically shaped with its center stabilized inside the burner outlet.

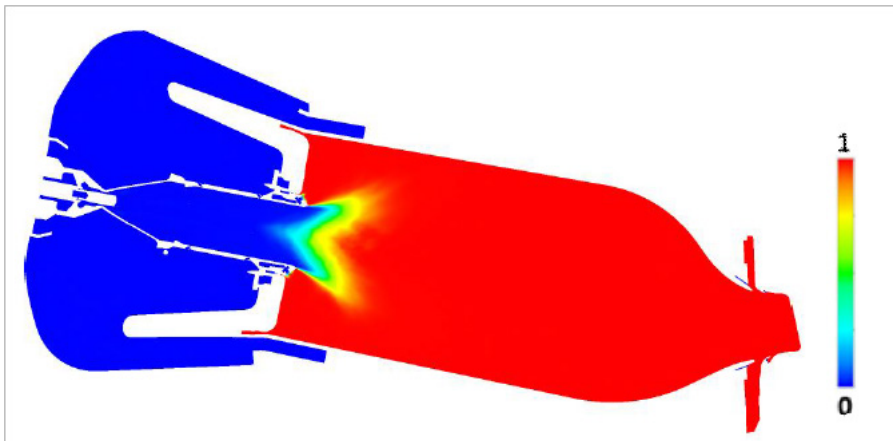


Figure 35. Time-averaged reaction progress in burner mid plane.

The corresponding temperature field, both a snapshot and the time average, are shown in Fig. 36. Here local structure of the main flame can be seen to be highly wrinkled by the turbulence and vortex break-down region associated with the burner exit region. The pilot flames are clearly seen close to the burner exit regions where the highest temperatures are found in Fig. 36. After approximately two burner diameters downstream the burner exit, most of the combustion is done and the temperature is evenly distributed before entering the turbine.

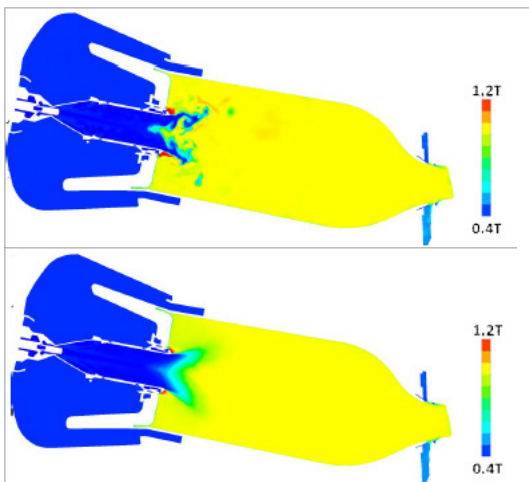


Figure 36. Instantaneous (top) and time averaged (bottom) temperature distributions in the burner.

### 5.2.2 Atmospheric case with hydrogen addition

Here the effect of hydrogen addition to an SGT-800 burner fitted to an atmospheric rig is studied using CFD and compared against measurement data. The result of hydrogen addition is presented in Fig. 37.

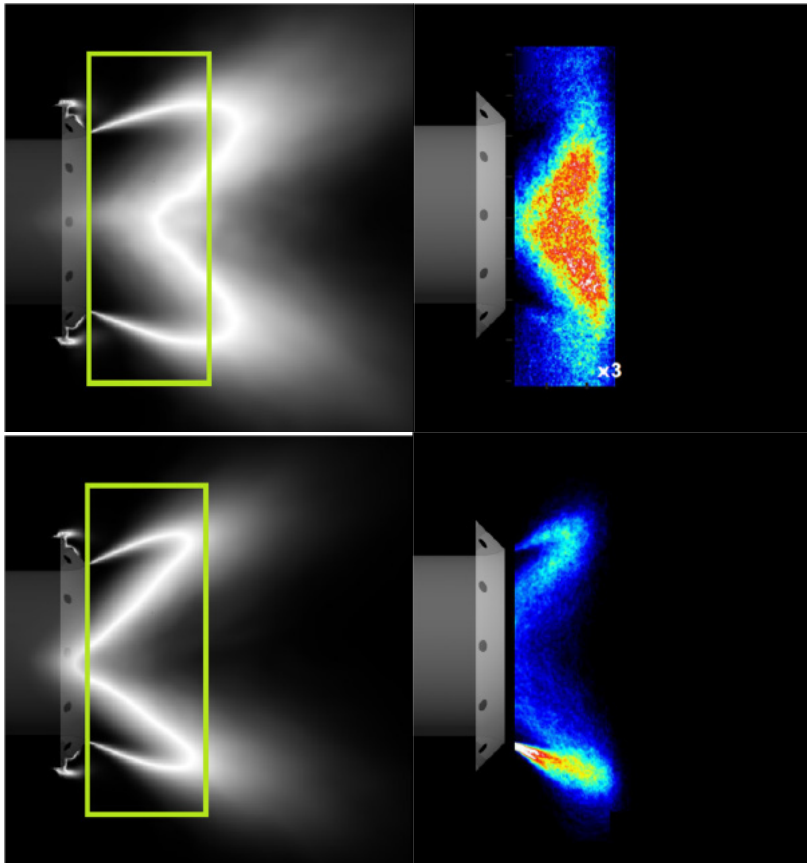


Figure 37. CFD results (left) compared with experimental data (right) of methane (top) and 20%methane + 80% hydrogen (bottom)

The CFD predictions show the time-averaged reaction progress where white represents a progress variable of 0.5 which is where the time-averaged position of the flame front will be. The experimental data are based on laser-induced fluorescence imaging of the OH radical where the gradient from the reactant side has been tracked and a probability density function of the gradient has been calculated. In the methane flame, the flame is situated outside of the burner most of the time. The flame is not fixed at one location, instead the flame seems to move around in the axial direction relative to the burner. For the hydrogen-enriched case the time average of the flame is situated much further upstream into the burner, which is seen in both CFD and the experimental data. It is also seen that the flame is much more concentrated close to its mean value which indicates the flame is not fluctuating in the axial direction as much as the pure methane flame is.

## 6 Conclusions

### 6.1 SUMMARY OF MAIN RESULTS

Determination of laminar burning velocity reveal decreasing trends with increasing pressure and increase with hydrogen addition, in fairly good agreement with common understanding. The highly interesting results are the combination of effects; suggesting that combustion enhancement by hydrogen addition is suppressed at fuel-rich conditions and elevated pressure.

Concentrations of species are in generally good agreement between experiments and modeling, thus the experimental results serve as a validation of the modeling approaches and put confidence in conclusions drawn from modeling.

The 4-step kinetic mechanism developed shows good agreement with more complex mechanism at lean conditions, with and without hydrogen addition, and is therefore a useful tool for implementation in CFD simulations, as exemplified in the gas turbine case presented in section 5. Here, predictions using both pure methane and hydrogen enriched methane are in good agreement with available experimental data.

Simulations of the laboratory setup was used as a comparison of mechanisms at different levels of complexity, and it is seen that the agreement is good between the reduced Z42 mechanism and the detailed GRI-Mech 3.0. The 4-step mechanism shows an overall good agreement but tends to overpredict the CO<sub>2</sub> concentration at distances 6-12 mm from the burner opening related to overprediction in temperature at the same position. This may be due to the insufficiently accurate resolution of the flame. Both the present 4-step and the Z42 mechanism predicts the position of the peak CO concentrations axially and radially correct. However, the present 4-step mechanism fails to predict the peak value of the CO concentration at all positions.

### 6.2 IMPLICATIONS FOR GAS TURBINE COMBUSTION

Gas turbine combustion is carried out at high pressure and an important motivation of this study was to experimentally investigate the combination of flame-suppressing effects at high pressure with flame-enhancing effects resulting from hydrogen addition.

The changes in flame behavior due to hydrogen addition are captured in the CFD, at least on a large-scale perspective. Knowledge on how the flame behavior is changing when increasing the hydrogen content is very important in gas turbine design since changes in flame shape and position is most often followed by secondary effects. Examples of secondary effects are wall heat load and turbine inflow condition which are both very important for the overall performance of a gas turbine.

### 6.3 OUTLOOK

The present study makes an important contribution to the understanding of flames at elevated pressures and hydrogen addition. Computational combustion research always has to compromise in a trade-off between time consumption and accuracy of results. The presented comparison of different kinetic mechanism serves as a foundation for selection of the best computational tools for continued studies. The experimental results have a two-fold use: they provide important fundamental understanding and they are used as validation of computational results.

The experimental setup used is new and has now been shown to have a large potential for further increasing the understanding of high-pressure combustion. The present project does not only produce unique experimental data; it also serves as a stepping stone towards further research. For continued work further development of the analysis of experimental results would be advantageous, including refinement of the method for estimating laminar burning velocities. These improvements would allow higher accuracy in evaluated species concentrations as well as a quantitative determination of laminar burning velocities.

## 7 References

1. S. Chu; A. Majumdar, *Nature* 488 (7411) (2012) 294-303.
2. E. J. K. Nilsson; J. Larfeldt; M. Rokka; V. Karlsson, *Energiforsk Report* 2015:121 (2015).
3. A. Konnov, in: *European Combustion Meeting, Budapest, Hungary* (2015).
4. S. S. Rashwan; M. A. Nemitallah; M. A. Habib, *Energy Fuels* 30 (12) (2016) 9981-10014.
5. A. Lantz; R. Collin; M. Alden; A. Lindholm; J. Larfeldt; D. Lorstad, *J Eng Gas Turb Power* 137 (3) (2015).
6. M. Andersson; J. Larfeldt; A. Larsson, *SGC Rapport* 2013:156 (2013).
7. E. J. K. Nilsson; A. van Sprang; J. Larfeldt; A. A. Konnov, *Fuel* 189 (2017) 369-376.
8. R. T. E. Hermanns; A. A. Konnov; R. J. M. Bastiaans; L. P. H. de Goey; K. Lucka; H. Kohne, *Fuel* 89 (1) (2010) 114-121.
9. P. Dirrenberger; H. Le Gall; R. Bounaceur; O. Herbinet; P. A. Glaude; A. Konnov; F. Battin-Leclerc, *Energy Fuels* 25 (9) (2011) 3875-3884.
10. E. J. Hu; Z. H. Huang; J. J. He; H. Y. Miao, *Int J Hydrogen Energy* 34 (20) (2009) 8741-8755.
11. F. H. V. Coppens; J. De Ruyck; A. A. Konnov, *Combust Flame* 149 (2007) 409.
12. W. K. Metcalfe; S. M. Burke; S. S. Ahmed; H. J. Curran, *Int J Chem Kinet* 45 (10) (2013) 638-675.
13. A. L. Sanchez; F. A. Williams, *Prog Energ Combust* 41 (2014) 1-55.
14. C. L. Tang; Y. J. Zhang; Z. H. Huang, *Renewable & Sustainable Energy Reviews* 30 (2014) 195-216.
15. C. L. Tang; Z. H. Huang; C. K. Law, *Proc Combust Inst* 33 (2011) 921-928.
16. M. Brower; E. L. Petersen; W. Metcalfe; H. J. Curran; M. Fueri; G. Bourque; N. Aluri; F. Guethe, *J Eng Gas Turb Power* 135 (2) (2013).
17. A. Larsson; N. Zettervall; T. Hurtig; E. J. K. Nilsson; A. Ehn; P. Petersson; M. Alden; J. Larfeldt; C. Fureby, *Energy Fuels* 31 (2) (2017) 1904-1926.
18. F. N. Egolfopoulos; N. Hansen; Y. Ju; K. Kohse-Hoinghaus; C. K. Law; F. Qi, *Prog Energ Combust* 43 (2014) 36-67.
19. G. Boudier; L. Y. M. Gicquel; T. J. Poinot, *Combust Flame* 155 (1-2) (2008) 196-214.
20. H. Pitsch, in: *Annual Review of Fluid Mechanics*, 2006; Vol. 38, pp 453-482.

21. B. Fiorina; R. Vicquelin; P. Auzillon; N. Darabiha; O. Gicquel; D. Veynante, *Combust Flame* 157 (3) (2010) 465-475.
22. V. Subramanian; P. Domingo; L. Vervisch, *Combust Flame* 157 (3) (2010) 579-601.
23. J. Janicka; A. Sadiki, *Proc. Combust. Inst.* 30 (2005) 537-547.
24. F. C. Marincola; T. Ma; A. M. Kempf, *Proc Combust Inst* 34 (2013) 1307-1315.
25. C. Duwig; K. J. Nogenmyr; C. K. Chan; M. J. Dunn, *Combust Theor Model* 15 (4) (2011) 537-568.
26. G. Bulat; W. P. Jones; A. J. Marquis, *Proc Combust Inst* 34 (2013) 3155-3164.
27. P. H. Joo; J. Gao; Z. Li; M. Aldén, *Rev Sci Instrum* 86 (3) (2015) 035115.
28. A. C. Eckbreth, *Laser diagnostics for combustion temperatures and species*, Bordon and Breach, Amsterdam, The Netherlands, 1996.
29. P. C. Miles, *Appl Optics* 38 (9) (1999) 1714-1732.
30. K. C. Utsav; J. A. Silver; D. C. Hovde; P. L. Varghese, *Appl Optics* 50 (24) (2011).
31. K. Kohse-Höinghaus; J. B. Jeffries, *Applied Combustion Diagnostics*, Taylor&Francis, New York, 2002.
32. F. Fuest; R. S. Barlow; J. Y. Chen; A. Dreizler, *Combust Flame* 159 (2012) 2533-2562.
33. Z. S. Li; J. Kiefer; J. Zetterberg; M. Linvin; A. Leipertz; X. S. Bai; M. Alden, *Proc Combust Inst* 31 (2007) 727-735.
34. N. Zettervall; C. Fureby; E. J. K. Nilsson, *Energy Fuels* 30 (11) (2016) 9801-9813.
35. W. P. Jones; R. P. Lindstedt, *Combust Flame* 73 (3) (1988) 233-249.
36. B. Franzelli; E. Riber; M. Sanjose; T. Poinsot, *Combust Flame* 157 (7) (2010) 1364-1373.
37. A. Abou-Taouk; I. Sigfrid; R. Whiddon; L. E. Eriksson, *Turbulence, heat and mass transfer* 7 (2012) 785-788.
38. K. V. Meredith; D. L. Black in: *AIAA*, Reno, Nevada, 2006; Reno, Nevada, 2006; pp 1-13.
39. C. K. Westbrook; F. L. Dryer, *Prog Energ Combust* 10 (1) (1984) 1-57.
40. N. Slavinskaya; M. Braun-Unkhoff; P. Frank, *J Eng Gas Turb Power* 130 (2) (2008).
41. O. A. Marzouk; E. D. Huckaby, *Engineering Applications of Computational Fluid Mechanics* 4 (3) (2010) 331-356.
42. I. V. Novosselov; P. C. Malte, *J Eng Gas Turb Power* 130 (2) (2008).

43. A. Abou-Taouk; S. Sadasivuni; D. Lörstad; L. E. Eriksson; ASME 2013.
44. A. Abou-Taouk. Optimization of chemical kinetics mechanisms and numerical simulations of industrial gas turbine burners. Gothenburg University, 2014.
45. A. Abou-Taouk; B. Farcy; P. Domingo; L. Vervisch; S. Sadasivuni; L. E. Eriksson, *Combust Sci Technol* 188 (1) (2016) 21-39.
46. V. Bykov; U. Maas, *Combustion Theory and Modelling* 11 (6) (2007) 839-862.
47. J. A. Van Oijen; F. A. Lammers; L. P. H. De Goey, *Combust Flame* 127 (3) (2001) 2124-2134.
48. P. D. Nguyen; L. Vervisch; V. Subramanian; P. Domingo, *Combust Flame* 157 (1) (2010) 43-61.
49. F. Frenklach ; H. Wang; C. L. Yu; M. Goldenberg; C. T. Bowman; R. K. Hanson; D. F. Davidson; E. J. Chang; G. P. Smith; D. M. Golden; W. C. Gardiner; V. Lissianski.
50. modeFRONTIER [www.modefrontier.com](http://www.modefrontier.com)
51. CHEMKIN PRO Reaction Design: San Diego, 2010.
52. R. J. Vanderbei, *Linear programming: Foundations and extensions*. Springer, New York, 2001.
53. ANSYS FLUENT, [www.ansys.com](http://www.ansys.com), 2013.
54. D. Lörstad; A. Ljung; A. Abou-Taouk, in: GT2016-57694, 2016.
55. D. Moëll; D. Lörstad; X.-S. Bai, *Flow Turbulence Combust.* 96 (2016) 987-1003.

## Appendix A

# Hydrogen addition to flames at gas turbine relevant conditions

## Final report – Infraseriv Höchst section

Authors: Dr.-Ing. Sirko Ogriseck

Contact:  
Infraseriv GmbH & Co. Höchst KG  
Dr.-Ing. Sirko Ogriseck  
Industriepark Höchst, C 526  
65926 Frankfurt am Main, Germany

**Table of contents**

<u>1</u>	<u>Introduction</u> .....	52
<u>2</u>	<u>Hydrogen at Industriepark Höchst</u> .....	52
<u>3</u>	<u>Description of the combined heat and power plant</u> .....	54
<u>4</u>	<u>Hydrogen co-firing at the CHP plant</u> .....	55
<u>5</u>	<u>Standards</u> .....	56
<u>6</u>	<u>Materials for hydrogen pipes</u> .....	57
<u>7</u>	<u>Measuring</u> .....	58
<u>8</u>	<u>Security and safety</u> .....	59
<u>9</u>	<u>Joule-Thomson effect of hydrogen at throttling devices</u> .....	60
<u>10</u>	<u>Literature</u> .....	62
<u>11</u>	<u>P&amp;ID of hydrogen injection station</u> .....	63

## 1. Introduction

About 55 to 60 million tons of hydrogen are required annually worldwide for fertilizer and ammonia production as well as synthesis processes. This hydrogen is produced in large-scale petrochemical processes from fossil or biological sources including gasification and electrolysis of water or aqueous solutions.

Most of the hydrogen that is currently available is obtained from the chemical industry, which has been producing, distributing, using and generating hydrogen for decades. Hydrogen is a starting product in processes such as the Haber-Bosch process and a by-product in other processes such as chlorine-soda electrolysis. The chemical industry therefore has extensive expertise in the use of hydrogen and plays a major role in the energy conversion and further utilization of hydrogen.

There are plans to co-fire some of the available by-product hydrogen in one of the three gas turbines in the combined heat and power plant at Industriepark Höchst. This report provides an overview of the planning and realization of a hydrogen mixing station.

## 2. Hydrogen at Industriepark Höchst

About 50 million m<sup>3</sup> of hydrogen is generated per year at Industriepark Höchst in Frankfurt as a byproduct at a chlorine-soda electrolysis plant that produces chlorine and caustic soda [1]. Hydrogen production varies depending on the plant's technical availability. The hydrogen is utilized in pharmaceutical and chemical production at Industriepark Höchst and the Frankfurt-Griesheim Industrial Park, in a trailer filling station for road vehicles (Figure 1), in a public fueling station for fuel cell vehicles (cars, buses) and as fuel in the combined heat and power plant that generates steam and electricity at the park.

The hydrogen is stored in a 10,000 m<sup>3</sup> gasometer at 70 mbar (Figure 1) and is fed into the 7 and 225 bar grids via a compressor station, where it is available for downstream processes at the site. The hydrogen from the 225 bar grid is compressed up to 900 bar pressure by a hydraulically driven, dry-running piston compressor and transported to the public station via a 1.7 km pipeline. The hydrogen stream is treated in washers, driers and active coal filters in the chlorine-soda electrolysis plant before being fed to the gasometer. The hydrogen is further conditioned at Infracerv as shown in Figure 2 before being fed into medium and high pressure grids. Gas quality is monitored continuously at the points labeled "Q" in Figure 2. Hydrogen is stored in bottles and buffer storage after the 254 bar compressor and the particle filter.



Figure 1: Hydrogen gasometer and trailer filling station at Industriepark Höchst

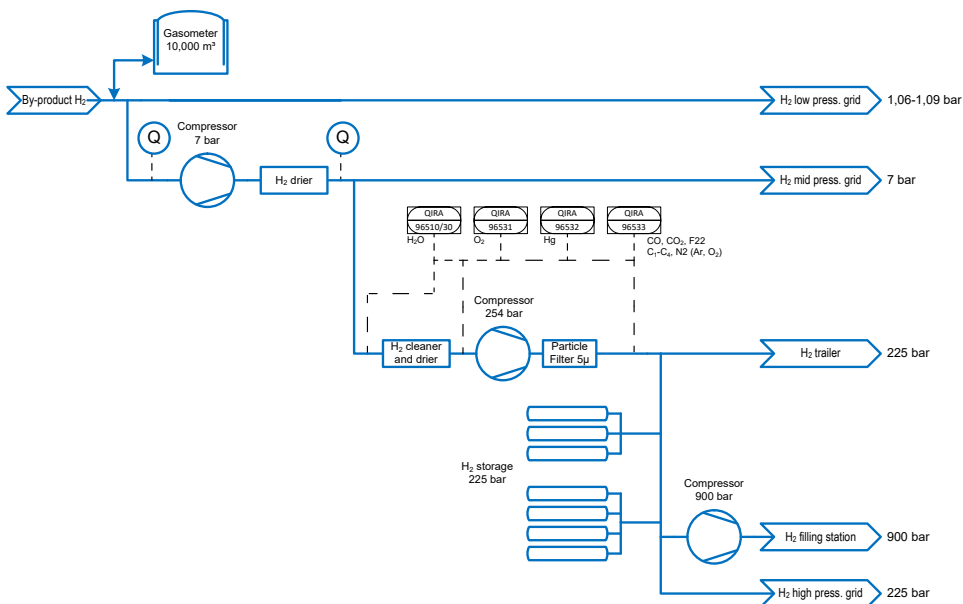


Figure 2: Hydrogen centre facility layout at Infracore

Table 1 shows the hydrogen quality measured at the trailer filling station. Hydrogen quality, particularly with regard to components such as Hg and moisture content, is also relevant for the safety of other components in the infrastructure (valves, storage, pipeline, etc.) and vehicles (storage tank). For other processes such as membrane technology for chlorine production, there does not exist any Hg impurity.

Table 1: Hydrogen quality available [2]

No.	Component	Measured values at Infraserb Höchst
1	CO	<1 ppmv
2	CO <sub>2</sub>	<1 ppmv
3	S compound	0
4	THC (C <sub>n</sub> H <sub>m</sub> )	<1 ppmv
5	O <sub>2</sub>	<2 ppmv
6	NH <sub>3</sub>	0
7	N <sub>2</sub> , Ar, He	<200 ppmv
8	H <sub>2</sub> O (G+L)	<1 ppmv
9	Na <sup>+</sup>	<0.01 ppmv
10	K <sup>+</sup>	<0.01 ppmv
11	Hg	<0.01 ppbv*
12	Particle	n.m.
13	Particle size	5 micro m filter

ppm = ppm (vol.), ppb = ppb (vol.); all values at normal conditions (NTP); n.m. = not measured

\* not relevant anymore because of change to membrane electrolysis

### 3. Description of the combined heat and power plant

Industriepark Höchst in Frankfurt am Main (Germany) has a combined heat and power (CHP) plant that supplies process and heating steam for the chemical, pharmaceutical and related process industries.

The plant consists of seven boilers with a collective steam capacity of 1,026 tons per hour. The two gas-fired boilers only burn natural gas, while the other two boilers burn hard coal, heating oil and natural gas. Heating oil is only a backup fuel. One of the gas-fired boilers is connected to the oxygen-rich exhaust gas of a gas turbine. A heat recovery steam generator installed at the site can recover heat from two gas turbines and use it to produce steam and hot water. There are also two high-voltage electrode boilers for steam production with a capacity of 20 MW each.

The live steam parameters are 121 bar and 515 °C. Both coal boilers make up the base load and basic power production sources. The two gas-fired boilers are used to meet intermediate and peak load requirements.

The live steam is reduced in steam turbines, which generate electricity. Three Siemens SGT-800 gas turbines (1x 45 MW and 2x 49 MW) are installed at the site. Taken together, the steam and gas turbines have an electricity generation capacity

of 260 MW. Part of the electricity that they produce is used directly by the combined heat and power plant to operate pumps, blowers and mills. However, Industriepark Höchst is supplied with external electricity as well.



Figure 3: Heat recovery steam generator with two Siemens SGT-800 turbines

#### 4. Hydrogen co-firing at the CHP plant

There are plans to co-fire hydrogen in one of the three gas turbines. Ideally, hydrogen will be taken from the 225 bar grid and reduced to the gas turbine inlet pressure for natural gas feeding. This requires the construction of a connection to the 225 bar grid. The hydrogen will be reduced and fed into the natural gas stream until the hydrogen content reaches 15 % vol. The gas turbine will then receive the mixed gas.

The hydrogen mixing system has to be designed and analyzed in detail to give due consideration to all applicable regulations and other literature on related subjects such as DVGW, BetrSichV, BImSchG, PED, et cetera. See chapter 5 for details.

Chapter 11 shows the P&ID for a possible hydrogen injection station to a natural gas pipeline.

A safety shut-off valve (with intermediate ventilation) is provided in the hydrogen line to prevent gas backflow and to stop the hydrogen flow. A backflow protection device (two check valves as self-operated regulators with differential pressure measurement and intermediate ventilation) is planned to be installed in the natural gas line to prevent hydrogen from back-flowing into the natural gas grid. This device is necessary if there is a possibility of the gas pressure in the line exceeding the gas pressure before the device. Coriolis mass meters may be considered to

measure hydrogen and natural gas mass flows. The desired ratio of hydrogen to natural gas is set via the flow controller. The pressure controller reduces the hydrogen to the gas turbine inlet pressure. A safety relief valve is provided. The isolating valves can be designed as ball valves with a double-block-and-bleed function.

The gas can be mixed in a tee section according to DVGW Standard G265-3 [2].

Planning/design and erection must be inspected by an independent expert for high pressure gas pipes.

## 5. Standards

National and international standards and regulations must be observed for hydrogen injection plants. In Germany, this includes DVGW standards such as G265-1 and G265-3.

Plant planning and execution must comply with all binding laws, regulations, technical rules, directives, codes, ordinances and standards. For hydrogen and natural gas systems, these include, without limitation:

- 2014/68/EU Pressure Equipment Directive (PED)
- DIN EN 14141 Valves for natural gas transportation in pipelines - Performance requirements and tests
- DIN 3230-5 Technical conditions of delivery of valves - Valves for gas installations and gas pipelines - Part 5: Requirements and tests
- ISO 3183 Petroleum and natural gas industries - Steel pipe for pipeline transportation systems
- API 941 Steels for hydrogen service at elevated temperatures and pressures in petroleum refineries and petrochemical plants
- IGC Doc 121/04/E Hydrogen transportation pipelines
- IGC Doc 121/14 Hydrogen pipeline systems
- IGC Doc 122/11/E Environmental impacts of hydrogen plants
- IGC Doc 15/06/E Gaseous hydrogen stations
- DVGW G 260 (A) Gas properties
- DVGW G 262 (A) Use of gases from renewable sources in public gas supply
- DVGW G 265-1 Stations for treatment and feed-in of biogas into gas supply networks – Part 1: Gases produced by fermentation - design, manufacture, installation, testing and commissioning
- DVGW G 265-3 (M) Plants for the injection of hydrogen into the gas grid; Planning, manufacturing, installation, testing, commissioning and operation
- DVGW G 463 (A) High pressure gas steel pipelines for a design pressure of more than 16 bar; Construction

- DVGW G 491 (A) Gas pressure regulating stations for inlet pressures up to and including 100 bar; Planning, manufacturing, installation, testing, commissioning and operation
- DVGW G 492 (A) Gas flow metering systems with an operating pressure up to and including 100 bar; Planning, manufacturing, installation, testing, commissioning, operation and maintenance
- German Technical Rules for Pipelines (Technische Regel für Rohrfernleitungsanlagen, TRFL)
- German Industrial Safety Regulation (Betriebssicherheitsverordnung, BetrSichV)
- German Pressure Vessel Regulation (Druckbehälterverordnung, DruckbehV)
- German Federal Immission Control Act (Bundesimmissionsschutzgesetz, BImSchG)

The absence of regulations and standards from this list does not exempt operators from complying with them as required by listed technical rules, directives, codes, ordinances or standards.

## 6. Materials for hydrogen pipes

### Piping

According to DVGW Standard G265-3, materials with tensile strengths exceeding 800 N/mm<sup>2</sup> must not be used in order to avoid hydrogen-induced stress-corrosion cracking [2]. Information on suitable materials can be found in sources such as IGC Doc 121/04 / E, IGC Doc 121/14, Technical Rules for Pipelines TRFL, DVGW G463, ISO 3183 or API 941.

Materials for hydrogen pipes and pipelines must meet the following requirements:

- Resistance to internal pressure
- Resistance to hydrogen
- Weldability
- Testability
- Availability of required semi-finished products
- Experience in application and processing
- Economically acceptable prices and delivery times.

Particular attention must be paid to the welding seams.

Any suitable steel (for example P235GH) can be used at ambient temperatures as long as the pressure remains 10 bar or less. The same steels used for natural gas could be also used for hydrogen. There have been no observations indicating that hydrogen has caused cracking or other material destruction in long-term operation.

There is a good material data base for the pressure range of 100 bar. When conditions exceed 200 °C and 200 bar, materials must be able to resist attack by hydrogen (H<sub>2</sub> embrittlement). Suitable materials include low-alloy steels (Cr, Mo) and especially austenitic steels.

Austenitic materials are recommended at pressures above 500 bar. The austenitic-ferritic material 1.4462 (duplex steel) is a suitable choice due to its high corrosion resistance and strength. It was used for the 1000 bar hydrogen pipeline at Industriepark Höchst. There are empirical data and test results for use with pressurized hydrogen as well as the necessary processing specifications.

Welding is the preferred connection method for obtaining dependable, leak-tight fittings. Screw couplings or terminals should only be used on a case-by-case basis. Screw connections, clamping ring screw connections or cutting ring fittings are generally suitable for hydrogen. The weld seams must comply with current specifications regarding accuracy, structure, weld root formation and surface quality. Care must be taken to obtain a round profile during welding.

Exterior corrosion poses the greatest danger to the pipes. Underground pipelines must be adequately protected from corrosion.

High-pressure seals with stainless steel inner flanges could be used as standard seals. Elastomers such as nitrile rubber (NBR) seals with a reinforcing metal ring and a gas rating are also possible for pressures of 10 bar or less. Generally, non-metallic seals are not suitable for pressurized hydrogen.

### **Valves**

All gas-rated valves can be used, provided they are resistant to stress-corrosion cracking and hydrogen embrittlement. Valves with bellow sealing will be provided. Valves should be connected to the pipes by welds, not flanges (except for start and end). A pressure and leak test is recommended.

## **7. Measuring**

The following instruments are used to measure hydrogen:

1. Coriolis mass flow meters
  - a. Simple instrument technology and small size
  - b. No moving parts
  - c. No or minimal requirements regarding the inlet and outlet section
  - d. Acceptable to the Office of Weights and Measures
  - e. Integrated density sensor
  - f. High pressure loss
  - g. Used up to 225 bar in the hydrogen grid at Industriepark Höchst
2. Turbine wheel gas meters

- a. Broad measurement range
  - b. Good long-term stability
  - c. An inlet and outlet section must be provided
  - d. Wear due to moving parts
  - e. Used in the low pressure 70 mbar hydrogen grid at Industriepark Höchst
3. Rotary displacement gas meters
- a. Utilized for low flow and ultra-low flow measurements
  - b. No requirements regarding the inlet and outlet section
  - c. Generates pulsations
  - d. Used up to 10 bar in the hydrogen grid at Industriepark Höchst
4. Differential pressure gas meters
- a. Rugged system
  - b. No moving parts
  - c. Only analog measurement signal
  - d. Require a large inlet and outlet section
  - e. Measurement uncertainties due to edge sharpness
  - f. Used up to 10 bar in the hydrogen grid at Industriepark Höchst

The same digital density volume converter that is used for natural gas could also be used for hydrogen.

## 8. Security and safety

In areas outside of Industriepark Höchst, vandalism can be prevented by fencing, camera surveillance, barriers, inspections and other appropriate measures. Mechanical safety equipment must be installed as well as technical shut-off mechanisms such as hydrogen supply shut-off, emergency stop, temperature and pressure monitoring, et cetera.

Hazardous areas are defined according to the applicable standards.

Safe separation distances from neighbor plants or residential / commercial areas must be maintained.

Pressure and temperature limits have to be defined during detailed planning.

Pipeline fires involving a natural gas/hydrogen mixture would have consequences comparable to fires in natural gas pipelines. There are significant differences between the fire behavior of pure hydrogen and that of natural gas. Pure hydrogen has almost no radiant heat and is not visible in daylight.

## 9. Joule-Thomson effect of hydrogen at throttling devices

The Joule-Thomson effect describes the behavior of a real gas during an isenthalpic state change. It is caused by the attraction and repulsion forces present in real gases. Throttling reduces the pressure, which increases the distance between the gas molecules. Work either has to be done if the attracting forces predominate, or work has to be released in the form of heat if the repulsion forces predominate.

During an adiabatic pressure reduction, this work can only be performed by the gas molecules. The negative acceleration work needed to overcome the attractive forces is achieved by decreasing the average molecular velocity, which is why the temperature decreases. When the repulsion forces predominate, the gas molecules are accelerated, which increases their mean molecular velocity and the temperature.

The mode of operation or direction of the differential Joule-Thomson effect is described by the Joule-Thomson coefficient  $\mu_{JT}$ :

$$\mu_{JT} = \left( \frac{\partial T}{\partial p} \right)_h. \quad (1)$$

If the Joule-Thomson coefficient is positive, an isenthalpic state change will lead to a temperature decrease. If pressure decreases, the change in pressure is negative, and the temperature change must also be negative in order to obtain a positive coefficient. The opposite is true for a negative Joule-Thomson coefficient. In this case, the temperature of the gas increases with isenthalpic throttling. The direction and magnitude of the temperature change of the Joule-Thomson effect depend on the temperature and the pressure.

Figure 4 shows the Joule-Thomson inversion curve where the Joule-Thomson coefficient is zero, i.e. temperature does not change. Within the curve, throttling leads to a cooling of the gas. Outside the curve, it leads to a heating of the gas. It is clear that the marked temperature range for hydrogen pressure reduction lies well outside the inversion curve. As a result, any isenthalpic restriction during pressure reduction leads to heating.

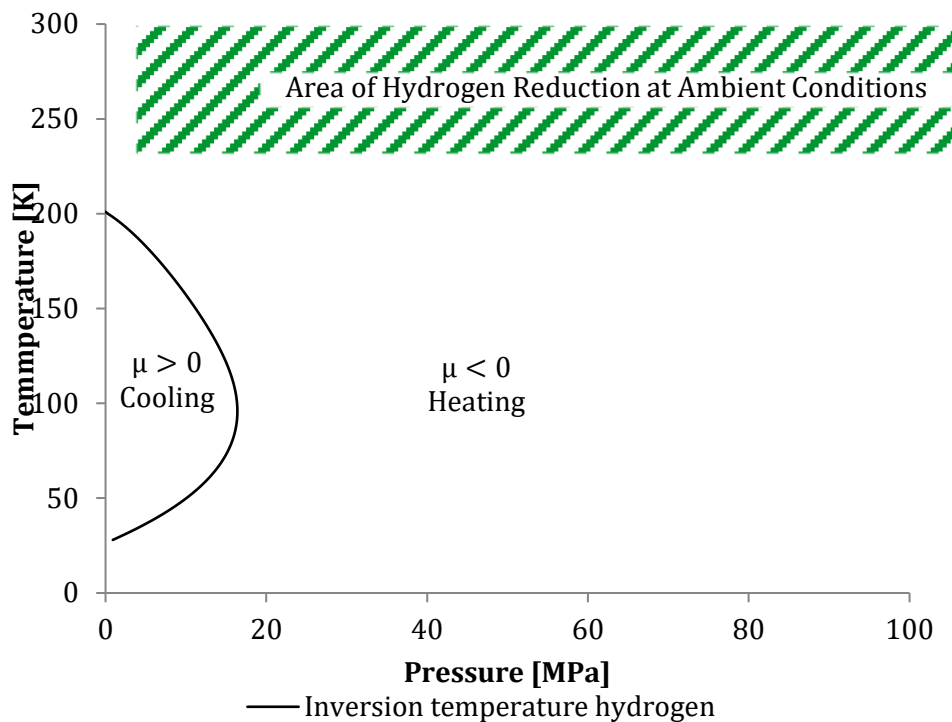


Figure 4: Joule-Thomson inversion curve and area of hydrogen reduction at ambient conditions

If throttling valves are used at ambient conditions, hydrogen will heat up when it is expanded at high pressures and ambient temperatures, Figure 5.

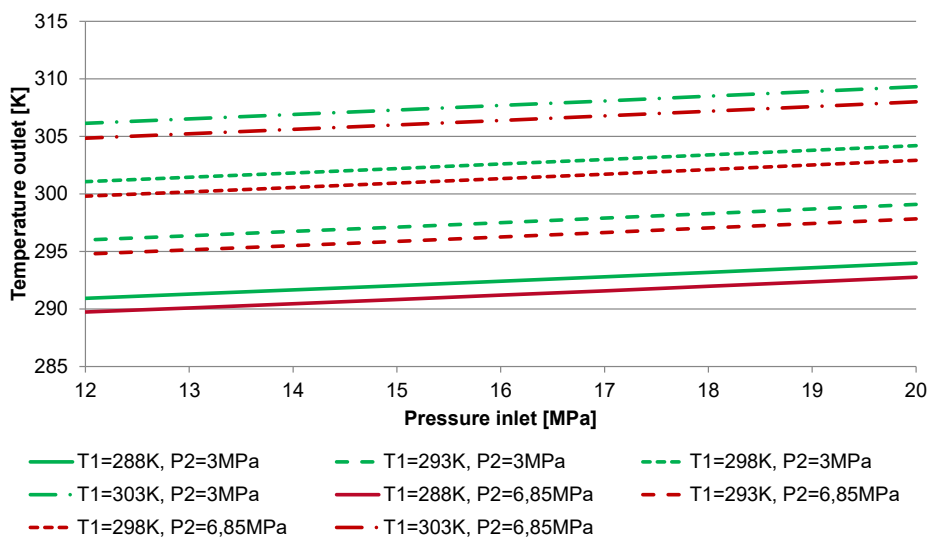


Figure 5: Outlet temperature after throttling valves at different ambient temperatures

## 10. Literature

- Baum, W. et al.: Auslegung, Bau und Betrieb von 5 MW und 20 MW Methanisierungsanlagen für das Energiespeicherkonzept ‚Power to Gas‘ - Eine Vorstudie, Final Report, FKZ 0325627, Infracore GmbH & Co. Höchst KG, Frankfurt am Main, Germany, 2014, <https://doi.org/10.2314/GBV:842184619>
- Rastogi, A. et al.: Chemical By-Product Hydrogen as an Alternative Motor Fuel, Proceedings Fuel Cell Seminar, Hawaii, 2006
- DVGW G 265-3 (M) Plants for the injection of hydrogen into the gas grid; Planning, manufacturing, installation, testing, commissioning and operation, ISSN 0176-3490, DVGW, March 2014



## Appendix B

Additional figures concerning the development of 4-step mechanism.

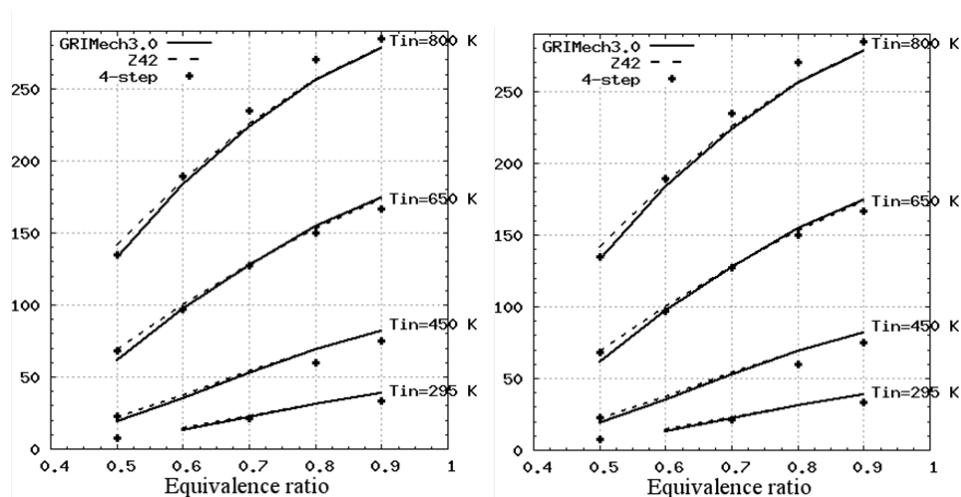


Figure B1. Burning velocity versus equivalence ratio,  $p=1\text{atm}$ . 20%. Left: CH<sub>4</sub>, 80% H<sub>2</sub>. Right: 40% CH<sub>4</sub>, 60% H<sub>2</sub>.

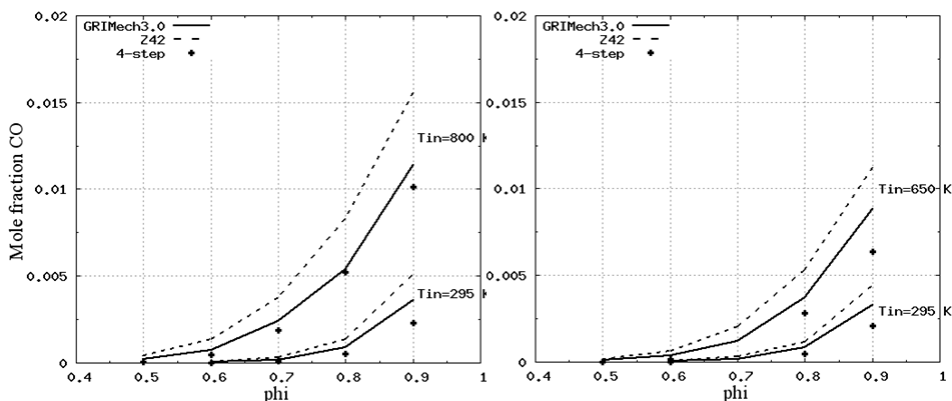


Figure B2. CO mole fraction vs. equivalence ratio, Left: 100% CH<sub>4</sub>, Right: 60% CH<sub>4</sub>.

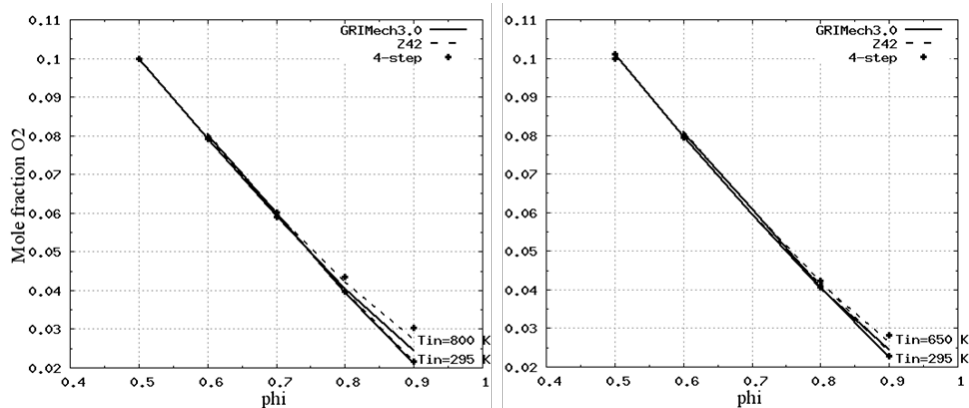


Figure B3. O<sub>2</sub> mole fraction vs equivalence ratio, Left: 100% CH<sub>4</sub>, Right: 60% CH<sub>4</sub>.

## Appendix C

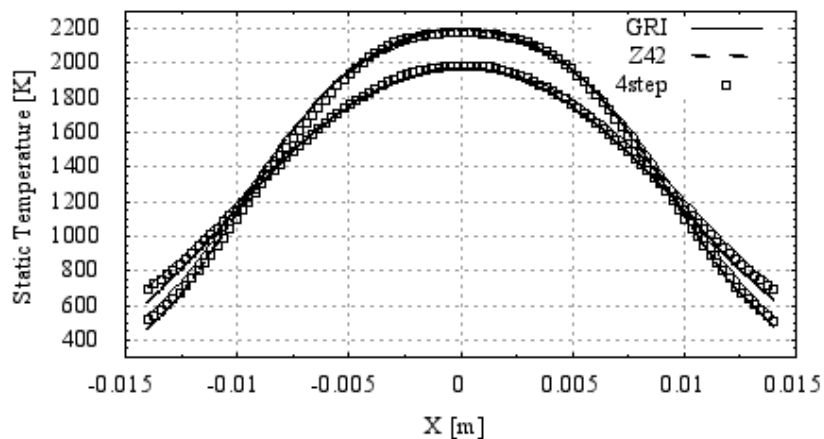


Figure C1. Static temperature at two positions with increasing distance from the burner opening. 19mm (bottom), and 35mm (top), 100% CH<sub>4</sub>.

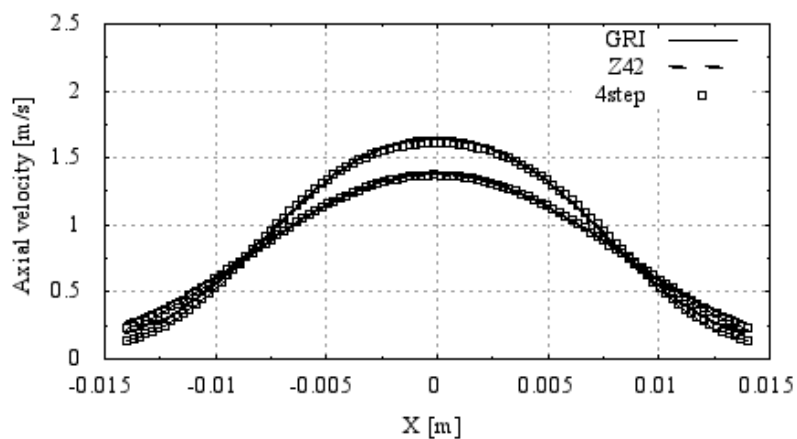


Figure C2. Axial velocity at two positions with increasing distance from the burner opening. 19mm (bottom), and 35mm (top), 100% CH<sub>4</sub>.

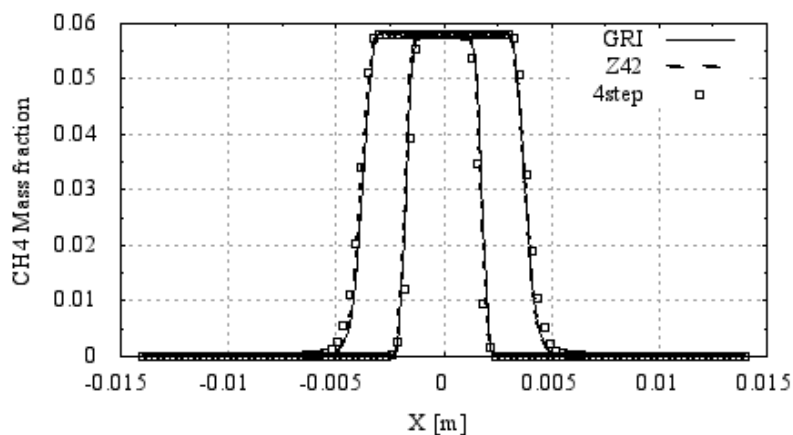


Figure C3. CH<sub>4</sub> mass fraction at two positions with increasing distance from the burner opening. 0mm (bottom) and 6mm (top line), 100% CH<sub>4</sub>.

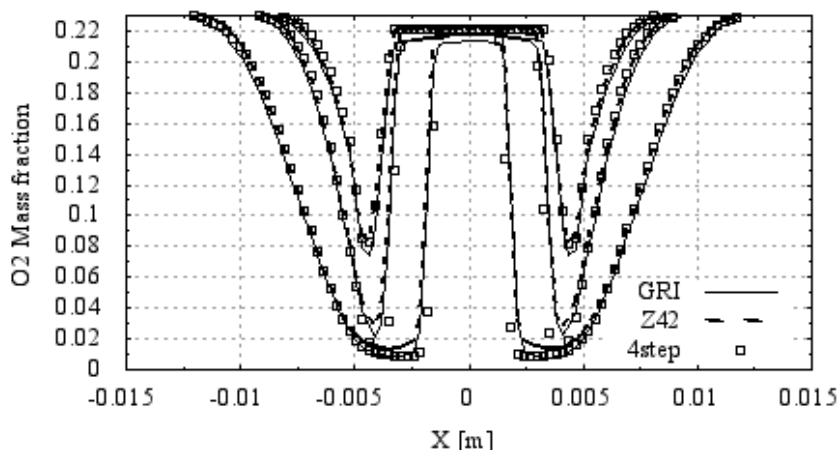


Figure C4. O<sub>2</sub> mass fraction at three positions with increasing distance from the burner opening. 0mm (bottom), 1mm (middle line) and 6mm (top line), 100% CH<sub>4</sub>.

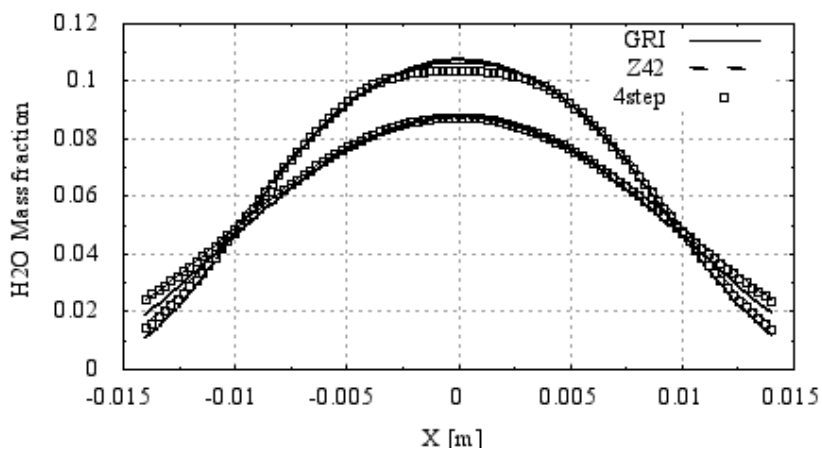


Figure C5. H<sub>2</sub>O mass fraction at two positions with increasing distance from the burner opening. 28mm (bottom), and 48mm (top), 100% CH<sub>4</sub>.

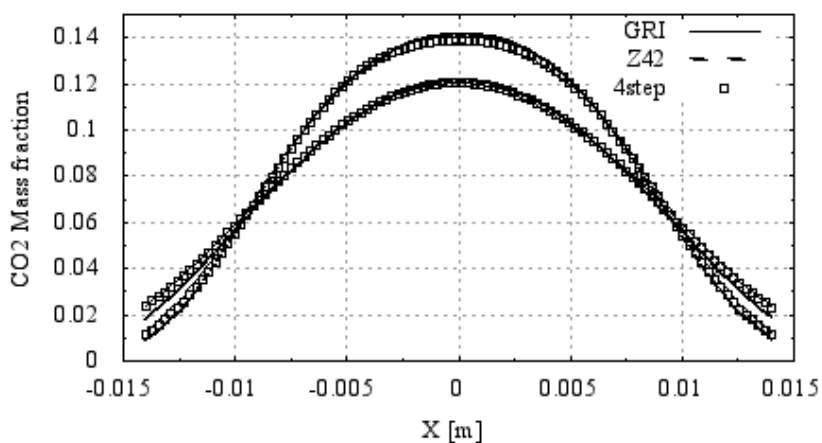


Figure C6. CO<sub>2</sub> mass fraction at two positions with increasing distance from the burner opening. 28mm (bottom), and 48mm (top), 100% CH<sub>4</sub>.



# HYDROGEN ADDITION TO FLAMES AT GAS-TURBINE-RELEVANT CONDITIONS

Flames of relevance to combustion in gas turbines have been studied using experimental and computational methods. The aim is to increase the understanding of how the combustion depend on fuel composition with respect to the components methane, ethane, propane and hydrogen.

The results can contribute to more fuel flexible and environmentally sustainable production of electricity from gas turbines. Experimental data obtained in a new high-pressure facility show how flame properties change with fuel composition and pressure, with an increase in laminar burning velocity as a result of hydrogen addition and a decrease as pressure increase. Simulation studies have resulted in evaluation of chemical mechanisms for combustion modeling. The experimental and computational studies presented in this report can contribute to continued development of fuel flexible and environmentally friendly energy production using gas turbines.

Energiforsk is the Swedish Energy Research Centre – an industrially owned body dedicated to meeting the common energy challenges faced by industries, authorities and society. Our vision is to be hub of Swedish energy research and our mission is to make the world of energy smarter!